Available online at www.sciencedirect.com
ScienceDirect
Lithos 92 (2006) 276–299
LITHOS
www.elsevier.com/locate/lithos

Temporal evolution of a long-lived syenitic centre: The Kangerlussuaq Alkaline Complex, East Greenland

Morten S. Riishuus [a,*], David W. Peate [b], Christian Tegner [a], J. Richard Wilson [a], C. Kent Brooks [c], Chris Harris [d]

[a] *Department of Earth Sciences, University of Aarhus, 8000 Århus C, Denmark*
[b] *Department of Geoscience, University of Iowa, 121, Trowbridge Hall, Iowa City, IA 52242, USA*
[c] *Geological Institute, University of Copenhagen, Øster Voldgade 10, 1350 Copenhagen K, Denmark*
[d] *Department of Geological Sciences, University of Cape Town, Rondebosch 7700, South Africa*

Received 4 May 2005; accepted 27 March 2006
Available online 6 June 2006

Abstract

We present new mineral and whole-rock compositions and Sr–Nd–Hf–Pb–O–H isotope data on samples from the Kangerlussuaq Alkaline Complex (~1000 km^2) in central East Greenland, part of the North Atlantic Igneous Province. This complex mainly consists of the Kangerlussuaq Intrusion but includes at least 13 separate satellite intrusions emplaced in the uppermost crust close to the unconformity between Archaean gneisses and overlying Palaeogene flood basalts. The complex is divided into (i) older satellite intrusions (~55–53 Ma) composed of multiple syenites and granites and minor gabbros and peridotites, (ii) the voluminous Kangerlussuaq Intrusion (~50 Ma), which displays a gradual transition from quartz syenites (nordmarkites) at the margin to nepheline syenites (foyaites) in the centre, and (iii) younger satellite intrusions (~47–45 Ma) of minor syenites, granites and diorites concentrated southeast of the Kangerlussuaq Intrusion. The complex displays a temporal evolution in which SiO_2 decreases (74–56 wt.%) and total alkalis (6–16 wt.%), amphibole Na+K content, $^{206}Pb/^{204}Pb_{meas}$, ε_{Ndi} and ε_{Hfi} (+3 to +11) increase from the older intrusions through the nepheline syenites. This is followed by a reversal to higher silica (62–73 wt.%) and lower total alkalis (9–12 wt.%), amphibole Na+K content, $^{206}Pb/^{204}Pb_{meas}$, ε_{Ndi} and ε_{Hfi} (−13 to +2) in the younger satellite intrusions.

Temporal changes in the location of magma plumbing systems and in magma production rates played a profound role in controlling silica content, alkalinity and degree of crustal contamination during development of the complex. Phonolitic magma was only generated after prolonged magmatism had shielded the conduits from interaction with country rock. The parental magmas were probably basanitic to alkali olivine basaltic in composition. The older satellite intrusions and the Kangerlussuaq Intrusion have low $\delta^{18}O$ magma values (−1 to +6‰) compared to the younger, more crustally contaminated, satellite intrusions (+4.5 to +7‰). It appears that the magmas only had sufficient over-pressure to intrude the basalt cover when larger volumes of less contaminated trachyte magma were produced, resulting in the generation of low-$\delta^{18}O$ magmas due to dehydration of hydrothermally altered basalt xenoliths.

Keywords: Syenite; Isotopes; Assimilation; Plumbing system; Alkaline magmatism; East Greenland

* Corresponding author. Presently at: Department of Geological and Environmental Sciences, Stanford University, Stanford, CA 94305, USA. Tel.: +1 650 723 0841; fax: +1 650 723 2199.
E-mail address: riishuus@pangea.stanford.edu (M.S. Riishuus).

0024-4937/$ - see front matter © 2006 Elsevier B.V. All rights reserved.
doi:10.1016/j.lithos.2006.03.037

1. Introduction

The East Greenland portion (Fig. 1a) of the Palaeogene North Atlantic Igneous Province (e.g., Saunders et al., 1997) includes a post-break-up magmatic phase that occurred after extrusion of the voluminous tholeiitic Plateau Basalts (Larsen et al., 1989; Pedersen et al., 1997; Tegner et al., 1998b) at 56–54 Ma. A large part of this younger magmatic activity is concentrated at ~50–47 Ma, and it has been inferred to originate from passage of the rifted margin over the Iceland plume axis (Tegner et al., 1998a). This post-break-up phase includes significant volumes of alkaline magmatism that, at the present erosion level, are overwhelmingly dominated by felsic intrusions relative to lavas and mafic intrusions (e.g., Nielsen, 1987). More than 30 complexes exist, and they consist of silica under-saturated syenites, saturated syenites, quartz syenites, granites and quartz porphyries.

In this paper we focus on the petrology and geochemistry of the Kangerlussuaq Alkaline Complex (KAC) which is the largest Palaeogene intrusive complex in East Greenland. The KAC includes silica

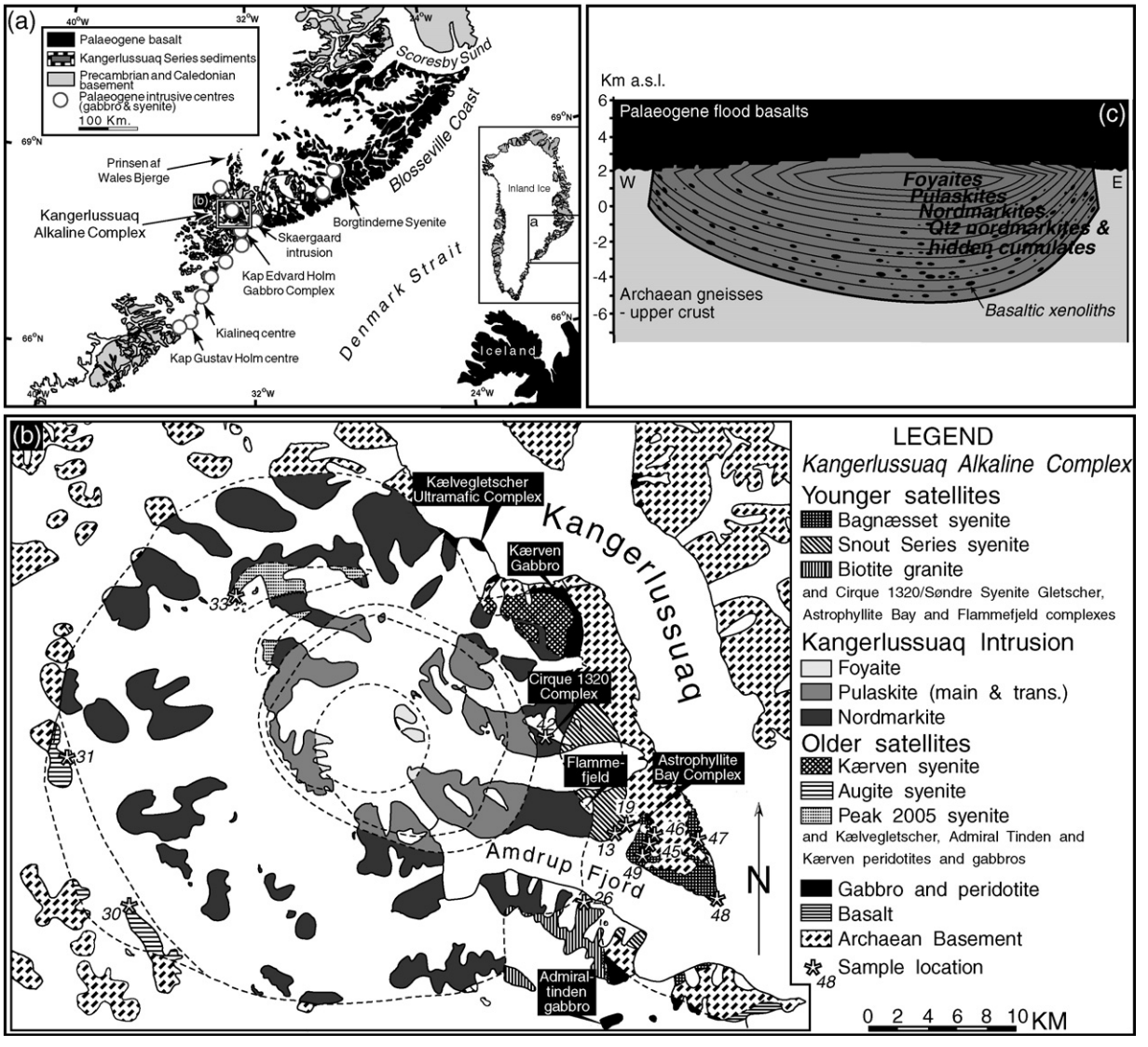

Fig. 1. (a) Map of Central East Greenland showing the distribution of Palaeogene flood basalts, intrusive centres (gabbros and syenites), the Kangerlussuaq sedimentary basin, and the Precambrian basement. (b) Map of the Kangerlussuaq Alkaline Complex west of Kangerlussuaq Fjord (after Kempe et al., 1970). Sample locations are indicated by asterisks. (c) Idealised cross-section through the Kangerlussuaq Intrusion from Riishuus et al. (submitted for publication-b), modified after Wager (1965).

over- and under-saturated syenites emplaced over an ~8 m.y. time period from ~53 to ~45 Ma. In this respect, it is distinct from most contemporaneous, felsic complexes in East Greenland that are either dominantly saturated to over-saturated (e.g., the Kialineq (Brooks, 1977; Brown and Becker, 1986) and Kap Gustav Holm centres (Myers et al., 1993)) or under-saturated (Borgtinderne Syenite; Brown et al., 1978). Many alkaline complexes are characterised by early, marginal quartz syenites and late, central nepheline syenites (e.g., Abu Khruq Complex, Egypt (Landoll et al., 1994); Mount Brome Alkaline Complex, Quebec (Chen et al., 1994); Messum Igneous Complex, Namibia (Harris et al., 1999)). The Kangerlussuaq Intrusion, dominating the KAC, is a classic example of such a structure (e.g., Wager, 1965). The KAC as a whole, however, differs from this pattern, as the youngest intrusions are over-saturated (e.g., Deer and Kempe, 1976). We will show that compositions and volumes of the KAC alkaline magmas changed with time, and we will try to relate these variations to petrogenetic processes, such as crustal assimilation and magma mixing, and the tectonic evolution of the region.

2. Overview of the Kangerlussuaq Alkaline Complex

The KAC comprises the ~50 Ma Kangerlussuaq Intrusion and a number of older and younger satellite intrusions (Fig. 1b). The geology and geochronology of the intrusions that constitute the KAC are summarised in Table 1 and discussed in the following sections.

2.1. The Kangerlussuaq Intrusion

The Kangerlussuaq Intrusion, which is roughly circular in outline (30–35 km in diameter), represents ~80% of the exposed area of the KAC (Table 1). It grades from foyaites (nepheline syenite, >5% feldspathoids) in the centre, through main pulaskites (mildly under-saturated syenite, <5% feldspathoids) and transitional pulaskites (saturated syenite with neither quartz nor feldspathoids), to nordmarkites (over-saturated syenite, <10% quartz) and outermost quartz nordmarkites (quartz-rich syenite, ~10% quartz) (Fig. 1b) (Wager, 1965). The intrusion was emplaced at the unconformity between the Archaean gneisses and the overlying flood basalts (Wager, 1965). An asymmetric, lopolithic form is suggested (Riishuus et al., submitted for publication-b) (Fig. 1c). Trains of huge, elongated, basaltic xenoliths (up to hundreds of metres) dipping 30–60° towards the centre of the intrusion are prominent in the nordmarkites and quartz nordmarkites. They are thought to have sunken to the transient floor of the magma chamber (Fig. 1c) (Wager, 1965). The quartz nordmarkites locally show modal layering, and lamination of platy feldspars in the nordmarkites and pulaskites dip 30–60° towards the centre. These structures imply a layered intrusion with a stratigraphic section from base to top.

As is typical of layered mafic intrusions, the Kangerlussuaq Intrusion formed from a complex interplay of magma injection, crustal assimilation and crystallisation. In a recent Sr–Nd–Hf–Pb isotope study (Riishuus et al., submitted for publication-b) we have suggested that the magmas emplaced into the Kangerlussuaq Intrusion chamber originated in a larger, underlying chamber, stratified from basanitic/alkali basaltic to phonolitic mantle-derived magma that interacted with crust in the roof zone. The presence of alkaline mafic material under the KAC is supported by occurrences of kaersutite gabbroic inclusions in dykes around the KAC (Brooks and Platt, 1975) and a large positive aeromagnetic anomaly (Verhoef et al., 1996; Riishuus et al., submitted for publication-b). Tapping from the roof zone of the master chamber resulted in emplacement of highly contaminated (~20% crust) nordmarkitic magma at the base of the flood basalts. Repeated recharge into the shallow chamber of the Kangerlussuaq Intrusion of less contaminated and less evolved phonolite from increasingly deeper parts of the roof zone in the underlying chamber, with progressive armouring, resulted in the formation of successively more primitive and less crustally contaminated syenites, ultimately reaching foyaite.

The $\delta^{18}O$ values of quartz (+0.7‰ to +4.6‰), alkali feldspar (−0.5‰ to +6.0‰) and amphibole/pyroxene (−2.4‰ to +3.4‰) from the Kangerlussuaq Intrusion reflect O-isotope equilibrium at magmatic temperatures with no or very little subsolidus alteration. These data suggest crystallisation from a magma depleted in ^{18}O relative to the mantle (Riishuus et al., submitted for publication-a). In particular, the low magma $\delta^{18}O$ values estimated for the nordmarkites (−1 to +4‰) were produced by dehydration of basaltic xenoliths that were hydrothermally altered by meteoric water prior to their capture in the magma chamber by stoping. The increased water pressure due to dehydration of these xenoliths lowered the liquidus temperature, resulting in the production of superheated magma, and possibly aided differentiation across the thermal barrier in the petrogenetic residual system by recharge with phonolite (Riishuus et al., submitted for publication-a).

Table 1
Summary of petrography, age, areal extent and field relations from the Kangerlussuaq Alkaline Complex, East Greenland

Intrusion	Rock type(s)	Age (Ma)	Location	Area %	km^2	Field relations	Source
Younger satellite intrusions							
Flammefjeld complex	Quartz porphyry breccias, Mo deposit	~40	E part of KI in nordmarkite	<1	~0.5	Breccia pipe, intruded by qtz porphyries, hydrothermal alteration	1–2
Cirque 1320 Complex [a]	Gabbro, diorite	–	E part of KI in nordmarkite	<1	~0.5	sub-volcanic plug sulphide mineralisation	3–5
Søndre Syenite Gletscher Granite Complex	Granite, monzonite	–	E part of KI in nordmarkite	<1	~0.5		6
Snout Series Syenite [a]	Syenite	45–47	E of KI	~3.5	~35	Some basaltic xenoliths	4–5, 7–9
Biotite Granite [a]	Biotite granite	~46	SE of KI	~3.5	~35		4–5, 7, 9
Astrophyllite Bay Complex [a]	Syenite, diorite, trachyandesite pillows	~47	E of KI	<1	~0.5	Diorite plug in syenite, gneissic xenoliths in syenite	4–5, 10–11
Bagnæsset Syenite Complex [a]	Syenite, granite	~47	E of KI	~1.5	~15	Frequent gneissic xenoliths, some basaltic xenoliths	4–5, 7, 12
Kangerlussuaq Intrusion [a] (KI)	Nordmarkite pulaskite foyaite	~50		~80	~800	Layered, lopolithic intrusion, frequent basaltic xenoliths, very few gneissic xenoliths	4, 9, 13–20
Older satellite intrusions							
Augite Syenite [a]	Augite syenite, monzonitic syenite, olivine gabbro	–	WSW of KI	~3.5	~35	Frequent basaltic xenoliths	5, 7
Peak 2005 Syenite [a]	Syenite	–	NW part of KI	~2	~20		5, 7
Kærven Syenite Complex [a]	Syenite, granite	~53	NE of KI	~1	~10	Some gneissic and basaltic xenoliths	7, 9, 21–25
Kærven Gabbro	Layered gabbro	53–55	NE of KI	<1	~5		7, 9, 26–29
Admiraltinden Gabbro	Gabbro	–	SE of KI	~2	~20		7
Kælvegletscher ultramafic complex	Peridotite	–	NE of KI	~2	~20		30–31

[a] Compositional data from these intrusions are presented in this paper; Location, see Fig. 1b; (1) Geyti and Thomassen (1984); (2) Brooks et al. (2004); (3) Brooks et al. (1987); (4) Nielsen (2002); (5) this study; (6) Dahlstrøm (1989); (7) Deer and Kempe (1976); (8) Pedersen (1989); (9) Tegner et al. (submitted for publication); (10) Nielsen and Brooks (1991); (11) Riishuus et al. (2005); (12) Larsen (1982); (13) Wager (1965); (14) Kempe et al. (1970); (15) Kempe and Deer (1970); (16) Kempe and Deer (1976); (17) Pankhurst et al. (1976); (18) Brooks and Gill (1982); (19) Riishuus et al. (submitted for publication-b); (20) Riishuus et al. (submitted for publication-a); (21) Holm and Prægel (1988); (22) Nielsen (1989); (23) Holm and Prægel (1989); (24) Holm et al. (1991); (25) Holm (1991); (26) Ohja (1966); (27) Breddam (1995); (28) Skovgaard (1996); (29) Holm et al. (2006-this volume); (30) Prægel and Holm (2001); (31) Holm and Prægel (2006-this volume).

2.2. The older satellite intrusions

Based on field relations and limited geochronology, six minor satellite intrusions (Kælvegletscher Ultramafic Complex, Admiraltinden Gabbro, Kærven Gabbro Complex, Kærven Syenite Complex, Augite Syenite, Peak 2005 Syenite; Fig. 1b) are recognised as older than the Kangerlussuaq Intrusion (Table 1).

The Kælvegletscher Ultramafic Complex is composed of dunitic cumulates that have been suggested to represent a dynamic magma chamber with periods of replenishment, contamination and fractional crystallisation with a parental magma of tholeiitic affinity (Prægel and Holm, 2001; Holm and Prægel, 2006-this volume). The Admiraltinden Gabbro (Deer and Kempe, 1976) is, to our knowledge, essentially unstudied. The Kærven Gabbro Complex consists of several intrusive units with hypersthene gabbro as the most abundant rock type (Ohja, 1966; Deer and Kempe, 1976; Breddam, 1995). The gabbros of Kærven are cut by the Kærven Syenite Complex which was emplaced as multiple intrusions that young westwards (Holm and Prægel, 1988; Holm et al., 1991). Holm and Prægel (1988) concluded that this syenite–granite suite formed by fractional crystallisation of mantle-derived basaltic magmas with insignificant crustal contamination. Some

uncertainty exists about the exact age span of the units of the Kærven Gabbro and Syenite complexes (Holm, 1991), but recent biotite and amphibole Ar–Ar (Tegner et al., submitted for publication) and baddeleyite and zircon U–Pb (Holm et al., 2006-this volume) dating indicates a time interval from ~55 to ~53 Ma. The Augite Syenite, located west of the Kangerlussuaq Intrusion (Fig. 1b), differs from the other older syenite satellites by hosting abundant basaltic xenoliths and, according to Deer and Kempe (1976), shows evidence of an origin by digestion of basalt by syenitic magma. The Augite Syenite represents a gradational suite from olivine gabbro through monzonitic syenite to syenites with interstitial quartz that resemble the nordmarkites of the Kangerlussuaq Intrusion (Deer and Kempe, 1976). Unfortunately, the contact between the Augite Syenite and the Kangerlussuaq Intrusion is not exposed (Fig. 1b). Still, as basaltic xenoliths are very frequent in the cusp-shaped Augite Syenite relative to the nordmarkites immediately to the east, it seems plausible that it was emplaced as a circular-shaped body prior to the Kangerlussuaq Intrusion and stoped into the overlying basalts. Deer and Kempe (1976) described the Peak 2005 Syenite as a relatively fine-grained nordmarkite with marked compositional similarities to the nordmarkites of the Kangerlussuaq Intrusion by which it is engulfed.

2.3. The younger satellite intrusions

Based on field relations and limited geochronology, seven minor satellite intrusions (Astrophyllite Bay Complex, Bagnæsset Syenite Complex, Snout Series Syenite, Biotite Granite, Cirque 1320 Complex, Søndre Syenite Gletscher Granite Complex, Flammefjeld Complex; Fig. 1b) are recognised as being younger than the Kangerlussuaq Intrusion (Table 1).

The Astrophyllite Bay Complex consists of a small alkaline diorite plug with dislodged trachyandesitic pillows hosted by a matrix of co-magmatic syenite emplaced in the Archaean basement (Nielsen and Brooks, 1991; Riishuus et al., 2005). The syenite contains gneissic xenoliths showing varying degrees of anatexis. Both the diorite and the syenite formed from mantle-derived alkaline basaltic melts after prolonged assimilation–fractional crystallisation processes in separate magma chambers (Riishuus et al., 2005). The syenites and diorite were eventually emplaced as separate magma pulses in the same chamber. This gave rise to superimposed local contamination between, respectively, trachyandesitic melt pillows and the trachyte magma, and the trachyte magma and the surrounding gneisses. The age of the diorite intrusion is 47.1±0.7 Ma (Rb–Sr isochron age, Riishuus et al., 2005). The Bagnæsset Syenite Complex consists of dome- and sheet-forming nordmarkitic syenite with numerous gneissic and some basaltic xenoliths (Deer and Kempe, 1976; Larsen, 1982). Deer and Kempe (1976) originally designated the Bagnæsset Syenite Complex as an older satellite, but subsequent work has shown that the Astrophyllite Bay Complex is related to the Bagnæsset Syenite Complex (Larsen, 1982; Nielsen, 2002). Ar–Ar ages (Tegner et al., submitted for publication) are 45–47 Ma for the Snout Series Syenite (amphibole) and ~46 Ma for the Biotite Granite (biotite). The small Cirque 1320 Complex consists of a gabbroic to dioritic plug, with noteworthy sulphide mineralization, emplaced in the Kangerlussuaq Intrusion (Brooks et al., 1987; Goodwin and Turner, 1988). The Søndre Syenite Gletscher Granite Complex, possibly part of the Cirque 1320 Complex, consists of granites and monzonites (Dahlstrøm, 1989). The youngest activity in the KAC appears to be the sub-volcanic Flammefjeld Complex with quartz porphyry breccias hosting Mo, Pb, Zn, Ag and Au mineralization (Geyti and Thomassen, 1984). A 39.7±0.2 Ma molybdenite Re–Os age was determined by Brooks et al. (2004).

3. Samples and analytical techniques

This study is based on new compositional data and a compilation of previously published data (Holm and Prægel, 1988; Holm, 1991; Riishuus et al., 2005, submitted for publication-a,b) from 9 out of 14 intrusions belonging to the KAC (Table 1). We present new data on 19 samples from the Augite Syenite ($n=2$), Peak 2005 Syenite ($n=1$), Snout Series Syenite ($n=3$), Biotite Granite ($n=1$), Cirque 1320 Complex ($n=2$), Astrophyllite Bay Complex ($n=3$) and Bagnæsset Syenite Complex ($n=7$).

Pyroxene and amphibole compositions were determined with a JEOL JXA-8600 Superprobe at the Department of Earth Sciences, University of Aarhus. Major and trace element analyses on 16 whole-rock samples were carried out by X-ray fluorescence using a Phillips PW-2400 spectrometer at the Department of Earth Sciences, University of Aarhus. The Sr–Nd–Hf–Pb isotope data were obtained at Geocenter Copenhagen. Sr isotopes were measured using a TIMS, and Nd, Hf and Pb isotopes were measured using a VG Elemental Axiom multi-collector ICP-MS. Oxygen and hydrogen isotope analyses were performed at the University of Cape Town using a Finnigan MAT252 mass spectrometer. The complete analytical details are given in Riishuus et al. (submitted for publication-a,b). The most relevant

data are summarised in Tables 2 (pyroxene compositions), 3 (amphibole compositions), 4 (whole-rock major element and radiogenic isotope compositions) and 5 (oxygen and hydrogen isotopes). A full set of analyses from the KAC is available by the senior author.

4. Classification and petrography

4.1. Classification

All samples from the Kangerlussuaq Intrusion are peralkaline and (Na+K)/Al ranges from 1.03 to 1.23 (Riishuus et al., submitted for publication-b). A distinct group in the phonolite field (SiO_2=56–58 wt.%) of the TAS-diagram (Fig. 2) are nepheline syenites (intermediate to the miaskitic and agpaitic types) and classify as foyaites according to mineralogy and texture. The main and transitional pulaskites define a small cluster in the trachyte field (SiO_2=63–65 wt.%) (Fig. 2), and they are

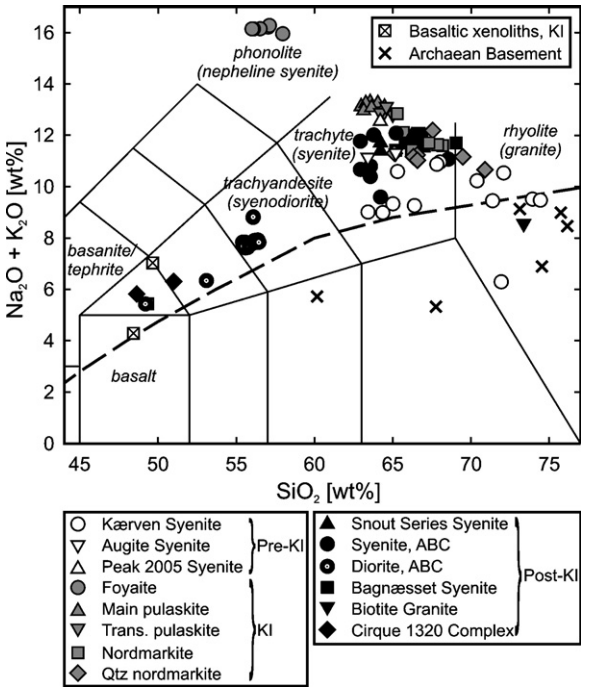

Fig. 2. Total alkalis–silica (TAS) classification diagram (Le Maitre, 1989) for whole-rock compositions of the Kangerlussuaq Alkaline Complex. Satellite intrusions older than the Kangerlussuaq Intrusion are shown in white, the Kangerlussuaq Intrusion in gray and the younger satellites in black symbols. The alkaline–tholeiitic division (dashed line) is from Irvine and Barager (1971). The data are from Holm and Prægel (1988), Holm et al. (1991) (Kærven Syenite Complex), Riishuus et al. (submitted for publication-b) (Kangerlussuaq Intrusion), Riishuus et al. (2005) (Astrophyllite Bay Complex) and this study (Augite Syenite, Peak 2005 Syenite, Cirque 1320 Complex, Bagnæsset Syenite Complex, Snout Series Syenite and Biotite Granite).

mildly under-saturated and saturated syenites, respectively. The nordmarkites and quartz nordmarkites plot in the trachyte field, except a few quartz nordmarkites that plot in the rhyolite field (SiO_2=65–71 wt.%), and are classified as (quartz) syenite, (quartz) alkali feldspar syenite and alkali feldspar granite after IUGS (Le Bas and Streckeisen, 1991).

The sample suite from the Kærven Syenite Complex (Holm and Prægel, 1988; Holm et al., 1991) varies in SiO_2 from 63 to 74 wt.% and spans the trachyte and rhyolite fields (Fig. 2). The main rock types are quartz syenite, alkali feldspar syenite and alkali feldspar granite, and both peralkaline and metaluminous varieties are present. The Augite Syenite (peralkaline), Peak 2005 Syenite (peralkaline), Snout Series Syenite (peralkaline/metaluminous) and Bagnæsset Syenite Complex (peralkaline/metaluminous) samples, and the felsic samples from the Astrophyllite Bay Complex (peralkaline/metaluminous) (Riishuus et al., 2005), all classify as syenite and (quartz) alkali feldspar syenite. The mafic rocks from the Cirque 1320 and Astrophyllite Bay complexes classify as gabbro, syeno-diorite and trachyandesite (melt pillows). All the syenitic satellite intrusions are alkaline in terms of total alkali and silica contents, except for the Biotite Granite (metaluminous) and some samples of the Kærven Syenite Complex (Fig. 2).

4.2. Petrography

The following summary of the petrography of the KAC samples is based on our observations together with those of Kempe and Deer (1970), Kempe et al. (1970), Larsen (1982), Holm and Prægel (1988), Holm et al. (1991) and Riishuus et al. (2005, submitted for publication-b).

4.2.1. The Kangerlussuaq Intrusion

The foyaites are medium grained, inequigranular and consist of 0.5–1.0-cm large, euhedral to subhedral, coarse microperthites (~60%) and interstitial clusters of euhedral to subhedral nepheline (25–30%), sodalite (0–8%), zoned aegirine augite (5–10%) and melanite garnet (0–4%). The pulaskites are coarse-grained inequigranular rocks, occasionally with 1.0–2.5-cm-large, euhedral, fine microperthite phenocrysts in the transitional pulaskites, with a groundmass of euhedral to anhedral, coarse microperthites (75–85%), interstitial plagioclase (~5%), and zoned sodic–calcic to sodic amphiboles (2–8%), aegirine augite (1–5%) and biotite (3–5%) in clusters with accessory titanite, FeTi-oxides and apatite. The transitional pulaskites contain neither visible quartz nor nepheline, whereas the main pulaskites show intergrowths of sodalite, nepheline and cancrinite in

Table 2
Selected average pyroxene compositions from the Kangerlussuaq Alkaline Complex, East Greenland

Sample	454046	454076	454076	454077	454077	454084	454089*	454089*	454047*	454110*	454062*	454111*	454067*	40325*	40329*	454027*	454029-B*
Intrusion	SS	AS	AS	AS	AS	PS	KIF	KI F	KI MP	KI TP	KI N	KI QN	KI QN	KS	KS	ABC Diorite	ABC Syenite
Mineral	a	sa	sa	sa	sa	aa	aa	aa	aa	aa	aa	aa	aa	a	hb	a	opx
Target		Core	Rim	Core	Rim		Core	Rim						Core	Core		
n	11	5	13	4	4	9	12	11	6	9	9	9	6			18	6
SiO_2	52.78	51.38	51.28	50.62	50.15	51.63	48.75	50.29	52.46	52.25	51.24	51.65	50.41	50.25	50.68	52.51	49.64
TiO_2	0.24	0.56	0.46	0.46	0.40	1.59	0.93	0.33	0.53	0.77	0.22	0.69	0.22	0.25	0.07	0.14	0.15
Al_2O_3	0.89	0.89	0.66	0.47	0.41	0.21	3.41	1.27	0.94	1.05	0.20	0.24	0.20	0.63	0.15	0.63	0.23
Cr_2O_3	0.01	0.01	0.00	0.00	0.01	0.01	0.01	0.00	0.01	0.01	0.01	0.00	0.01	0.01	0.00	0.00	0.00
FeOT	9.81	10.15	11.62	16.34	19.70	27.38	13.40	19.82	25.52	26.53	27.41	29.07	20.25	21.20	27.99	12.12	32.07
MnO	1.17	0.78	0.97	1.34	1.36	0.64	1.36	2.96	0.69	0.44	0.94	0.60	1.78	1.21	1.42	0.47	3.41
MgO	13.15	12.23	11.28	8.79	6.21	0.00	8.36	3.42	0.22	0.11	0.23	0.00	4.74	6.35	1.42	12.05	12.22
CaO	21.11	21.37	20.95	18.19	17.70	3.16	21.51	15.14	3.17	3.77	7.45	2.80	17.53	17.00	19.03	21.84	1.32
Na_2O	0.65	0.98	1.05	1.89	2.12	11.44	1.58	4.95	11.84	11.28	8.96	11.51	3.14	1.02	1.41	0.35	0.03
Total	99.81	98.35	98.27	98.11	98.05	96.05	99.30	98.18	95.37	96.20	96.65	96.58	98.28	97.92	102.17	100.12	99.07
Fe_2O_3	1.27	3.05	3.01	4.98	4.78	24.39	6.05	12.03	24.84	23.46	20.42	26.96	7.81	0.00	2.45	0.86	0.00
FeO	8.67	7.40	8.91	11.85	15.39	5.44	7.95	9.00	3.16	5.41	9.04	4.81	13.23	21.20	25.78	11.35	32.07
New total	99.94	98.66	98.58	98.61	98.53	98.49	99.91	99.38	97.86	98.55	98.70	99.28	99.06	97.92	102.42	100.21	99.07
Formula based on 6 oxygen atoms																	
Si	1.979	1.956	1.967	1.974	1.988	2.023	1.868	1.972	2.046	2.035	2.028	2.014	1.993	2.018	2.012	1.983	1.997
Ti	0.007	0.016	0.013	0.014	0.012	0.047	0.027	0.010	0.016	0.022	0.007	0.020	0.006	0.008	0.002	0.004	0.005
Al	0.039	0.040	0.030	0.021	0.019	0.010	0.154	0.059	0.043	0.048	0.009	0.011	0.009	0.030	0.007	0.028	0.011
Cr	0.000	0.000	0.000	0.000	0.000	0.000	0.000	0.000	0.000	0.000	0.000	0.000	0.000	0.000	0.000	0.000	0.000
Fe^{3+}	0.036	0.087	0.087	0.146	0.143	0.719	0.174	0.355	0.729	0.688	0.608	0.791	0.232	0.000	0.073	0.024	0.000
Fe^{2+}	0.272	0.236	0.286	0.387	0.510	0.178	0.255	0.295	0.103	0.176	0.299	0.157	0.437	0.712	0.856	0.358	1.079
Mn	0.037	0.025	0.032	0.044	0.046	0.021	0.044	0.098	0.023	0.015	0.032	0.020	0.060	0.041	0.048	0.015	0.116
Mg	0.735	0.694	0.645	0.511	0.367	0.000	0.477	0.200	0.013	0.007	0.013	0.000	0.280	0.380	0.084	0.678	0.733
Ca	0.848	0.872	0.861	0.760	0.752	0.133	0.883	0.636	0.132	0.157	0.316	0.117	0.742	0.731	0.809	0.884	0.057
Na	0.047	0.073	0.078	0.143	0.163	0.869	0.118	0.376	0.895	0.851	0.687	0.870	0.240	0.079	0.109	0.026	0.003
Total	4.000	4.000	4.000	4.000	4.000	4.000	4.000	4.000	4.000	4.000	4.000	4.000	4.000	4.000	4.000	4.000	4.000
En	37.2	34.9	32.4	25.7	18.5	0.0	24.5	10.2	0.7	0.3	0.7	0.0	14.0	19.6	4.2	34.2	36.9
Fs	17.5	17.5	20.3	29.0	35.3	47.8	24.3	38.2	45.1	46.4	48.0	49.5	36.6	38.7	49.4	20.0	60.1
Wo	42.9	43.9	43.3	38.2	38.0	6.9	45.3	32.5	7.0	8.3	16.2	6.0	37.3	37.6	40.9	44.5	2.9
Ac	2.4	3.6	3.9	7.2	8.2	45.3	6.0	19.2	47.2	45.0	35.1	44.5	12.1	4.1	5.5	1.3	0.1
Mg#	70.5	68.2	63.4	49.0	36.0	0.0	52.7	23.5	1.5	0.8	1.5	0.0	29.5	34.8	8.3	63.9	40.4

SS, Snout Series Syenite; AS, Augite Syenite; PS, Peak 2005 Syenite; KI, Kangerlussuaq Intrusion; F, foyaite; MP, main pulaskite; TP, transitional pulaskite; N, nordmarkite; QN, quartz nordmarkite; KS, Kærven Syenite; ABC, Astrophyllite Bay Complex; a, augite; sa, sodian augite; aa, aegirine augite; hb, hedenbergite; $Mg\# = 100 \times Mg/(Mg + Fe^{2+} + Fe^{3+})$; *n*, number of analyses. *Representative samples compiled from published and unpublished data: KI (Riishuus et al., submitted for publication-b), KS (Holm and Prægel, 1988) and ABC (Riishuus et al., 2005). Ferric iron concentrations have been calculated using Eq. (3) in Droop (1987).

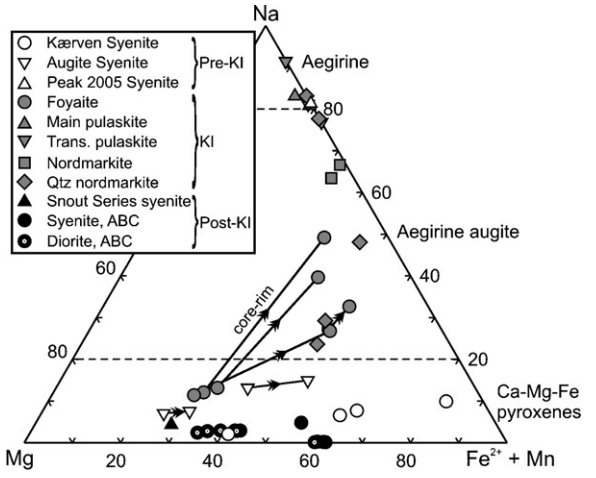

Fig. 3. Pyroxene compositions from the Kangerlussuaq Alkaline Complex shown in the Na–Mg–(Fe^{2+}+Mn) triangle. Tie-lines with arrows indicate compositional variations from core to rim. The data are from Holm and Prægel (1988) (Kærven Syenite Complex), Riishuus et al. (submitted for publication-b) (Kangerlussuaq Intrusion), Riishuus et al. (2005) (Astrophyllite Bay Complex) and this study (Augite Syenite, Peak 2005 Syenite and Snout Series Syenite).

interstitial pockets (0–5%). The nordmarkites are generally porphyritic with 0.5–3.0-cm-large phenocrysts of zoned, dark grey, euhedral to subhedral, fine microperthitic alkali feldspar plates in a medium-grained groundmass of subhedral to anhedral, coarse microperthites (75–90% total feldspar), and interstitial quartz (1–13%) in clusters with zoned sodic–calcic to sodic amphiboles (3–8%), aegirine augite (1–3%) and accessory plagioclase, FeTi-oxides, titanite, apatite, zircon and chevkinite.

4.2.2. The older satellite intrusions

The mineral assemblage of the Kærven Syenite Complex consists of euhedral, phenocrystic microperthite (60–80%), interstitial anhedral quartz (5–40%), dominantly calcic amphiboles (5–20%), augitic clinopyroxene (<5%), and minor plagioclase, Fe–Ti oxides, mica and olivine (occasional) plus accessory apatite and zircon. The Peak 2005 Syenite is porphyritic with euhedral, zoned, fine microperthite phenocrysts in a medium-grained groundmass of subhedral to anhedral coarse microperthite (~85% total feldspar), and interstitial strongly zoned sodic–calcic to sodic amphibole (~10%), aegirine augite (~5%), minor quartz and accessory FeTi-oxides, apatite, biotite and titanite. Deer and Kempe (1976) described large lithological variations in the Augite Syenite, from olivine gabbro to nordmarkitic syenite. Both coarse and fine- to medium-grained syenites occur, with euhedral to subhedral microperthite phenocrysts present in the latter. The principal constituents are microperthite (80–85%) and interstitial zoned sodic–calcic amphiboles (~8%), sodic

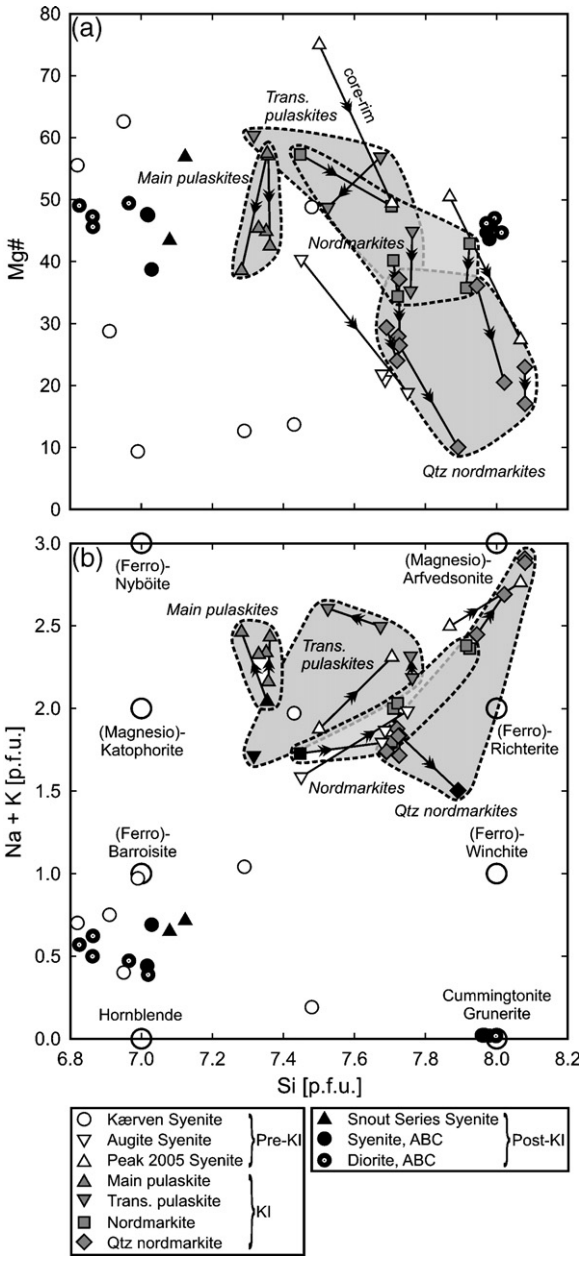

Fig. 4. (a) Mg# and (b) Na+K against Si for amphiboles from the Kangerlussuaq Alkaline Complex. Tie-lines with arrows indicate compositional changes from core to rim. Various amphibole end-member compositions (Leake et al., 1997) are shown for comparison. The data are from Holm and Prægel (1988) (Kærven Syenite Complex), Riishuus et al. (submitted for publication-b) (Kangerlussuaq Intrusion), Riishuus et al. (2005) (Astrophyllite Bay Complex) and this study (Augite Syenite, Peak 2005 Syenite and Snout Series Syenite).

augite (~3%), quartz (2–5%), FeTi-oxides (2–3%) and accessory apatite and titanite.

4.2.3. The younger satellite intrusions

The diorite plug in the Astrophyllite Bay Complex is medium grained and consists of plagioclase (55–60%), hornblende (20–33%), augite (0–12%), FeTi-oxides (2–8%) and biotite (2–5%), minor quartz and accessory apatite and zircon. The syenite is medium grained and contains alkali feldspars (75–80%), plagioclase (~10%), hornblende (2–5%), cummingtonite (2–5%), orthopyroxene (0–4%), quartz (2–3%), biotite (~1%) and accessory zircon, FeTi-oxides and chevkinite. The Bagnæsset Syenite Complex consists

Table 3
Selected average amphibole compositions from the Kangerlussuaq Alkaline Complex, East Greenland

Sample	454034	454046	454076	454076	454076	454077	454084	454084	454084	454084	454047*	454047*	454110*
Intrusion	SS	SS	AS	AS	AS	AS	PS	PS	PS	PS	KI MP	KI MP	KI TP
Mineral	mh	mh	fr	k	fr	fr	r	a	r	fr	mk	k	r
Target				Core	Rim		Core	Rim	Core	Rim	Core	Rim	Core
n	9	9	12	5	7	9	6	4	6	6	7	5	2
SiO_2	46.88	48.06	48.01	47.73	48.43	48.42	51.50	51.04	50.59	49.78	48.68	47.71	51.20
TiO_2	1.26	1.25	1.69	1.67	1.78	1.92	1.12	1.91	2.67	2.09	1.59	1.58	1.13
Al_2O_3	4.59	4.83	1.92	2.78	1.56	1.41	1.16	0.37	2.77	1.75	3.83	3.99	2.30
FeOT	21.44	16.50	27.01	21.41	27.71	27.37	17.87	23.98	9.31	17.76	15.40	19.78	15.65
MnO	1.35	1.20	1.25	1.14	1.22	1.38	1.42	2.00	0.80	1.29	1.93	2.22	1.92
MgO	9.24	12.20	4.02	8.15	3.64	4.29	10.21	5.09	15.66	9.81	11.47	8.20	11.58
CaO	9.37	10.45	5.63	7.52	4.65	5.44	3.13	1.58	7.21	4.55	5.49	3.91	3.24
Na_2O	1.82	2.05	5.25	4.54	5.60	5.18	7.51	8.14	5.88	6.98	6.46	7.21	7.70
K_2O	0.58	0.65	1.15	1.06	1.19	0.99	1.38	1.32	0.99	1.09	1.38	1.38	1.33
Total	96.54	97.20	95.95	96.00	95.79	96.42	95.33	95.42	95.89	95.12	96.24	95.97	96.05
Fe_2O_3	9.32	5.37	0.70	0.83	1.80	2.35	2.41	0.99	0.00	0.29	2.66	4.01	4.07
FeO	13.05	11.66	26.38	20.67	26.09	25.26	15.70	23.08	9.31	17.50	13.00	16.17	11.98
New total	97.47	97.74	96.02	96.08	95.97	96.66	95.57	95.52	95.89	95.15	96.50	96.37	96.46
Formula based on 23 oxygen atoms and assuming a total of 13 cations exclusive of Ca, Na and K													
Si	7.080	7.124	7.686	7.450	7.749	7.678	7.868	8.068	7.501	7.706	7.358	7.362	7.674
Al IV	0.817	0.844	0.314	0.512	0.251	0.264	0.132	0.000	0.484	0.294	0.642	0.638	0.326
Sum T	7.897	7.967	8.000	7.962	8.000	7.942	8.000	8.068	7.985	8.000	8.000	8.000	8.000
Al VI	0.000	0.000	0.049	0.000	0.044	0.000	0.077	0.069	0.000	0.024	0.041	0.087	0.080
Ti	0.143	0.139	0.204	0.196	0.214	0.228	0.129	0.227	0.298	0.244	0.181	0.183	0.128
Fe^{3+}	1.059	0.599	0.084	0.097	0.218	0.281	0.277	0.118	0.000	0.034	0.302	0.466	0.459
Mg	2.079	2.697	0.960	1.896	0.866	1.014	2.325	1.198	3.461	2.260	2.586	1.887	2.588
Fe^{2+}	1.649	1.446	3.533	2.699	3.492	3.349	2.006	3.052	1.154	2.268	1.643	2.087	1.502
Mn	0.069	0.118	0.170	0.113	0.166	0.127	0.184	0.268	0.086	0.170	0.247	0.290	0.243
Sum C	5.000	5.000	5.000	5.000	5.000	5.000	5.000	4.932	5.000	5.000	5.000	5.000	5.000
Fe^{2+}	0.000	0.000	0.000	0.000	0.000	0.000	0.000	0.000	0.000	0.000	0.000	0.000	0.000
Mn	0.103	0.033	0.000	0.038	0.000	0.058	0.000	0.000	0.015	0.000	0.000	0.000	0.000
Ca	1.521	1.662	0.966	1.258	0.796	0.926	0.513	0.268	1.144	0.752	0.890	0.647	0.520
Na	0.376	0.305	1.034	0.704	1.204	1.016	1.487	1.732	0.842	1.248	1.109	1.353	1.480
Sum B	2.000	2.000	2.000	2.000	2.000	2.000	2.000	2.000	2.000	2.000	2.000	2.000	2.000
Na	0.160	0.285	0.597	0.670	0.536	0.578	0.740	0.763	0.846	0.847	0.787	0.808	0.763
K	0.113	0.124	0.236	0.212	0.244	0.201	0.269	0.266	0.188	0.215	0.266	0.271	0.255
Sum A	0.273	0.410	0.833	0.882	0.780	0.779	1.009	1.029	1.033	1.062	1.052	1.079	1.017
Total	15.170	15.377	15.833	15.844	15.780	15.721	16.009	16.029	16.019	16.062	16.052	16.079	16.017
Mg#	43.4	56.9	20.9	40.4	18.9	21.8	50.4	27.4	75.0	49.5	57.1	42.5	56.9

SS, Snout Series Syenite; AS, Augite Syenite; PS, Peak 2005 Syenite; KI, Kangerlussuaq Intrusion; F, foyaite; MP, main pulaskite; TP, transitional pulaskite; N, nordmarkite; QN, quartz nordmarkite; KS, Kærven Syenite; ABC, Astrophyllite Bay Complex; mh, magnesiohornblende; fr, ferrorichterite; k, katophorite; r, richterite; a, arfvedsonite; mk, magnesiokatophorite; k, katophorite; ma, magnesioarfvedsonite; a, arfvedsonite; fb, ferrobarroisite; g, grunerite; $Mg\# = 100 \times Mg/(Mg+Fe^{2+}+Fe^{3+})$; *n*, number of analyses. *Representative samples compiled from published and unpublished data: KI (Riishuus et al., submitted for publication-b), KS (Holm and Prægel, 1988) and ABC (Riishuus et al., 2005). Ferric iron concentrations have been calculated using Eq. (6) in Droop (1987). Amphibole nomenclature is after Leake et al. (1997).

of coarse-grained nordmarkitic syenites with coarse perthites (80–90%), acmitic augite (~2%) mantled by hornblende (5–10%), interstitial quartz (1–5%), biotite (1–2%) and accessory chevkinite (up to 1–2%), titanite and apatite. The Snout Series Syenite hosts both equigranular medium-grained and porphyritic coarse-grained lithologies. Both varieties have coarse microperthites (~85%) and clusters of magnesiohornblende (~8%), interstitial quartz (3–5%), FeTi-oxides (<2%), minor augite and titanite, and accessory apatite, chevkinite, biotite and zircon. The Biotite Granite is medium grained and inequigranular, consisting of subhedral to anhedral perthite (~40%), subhedral zoned plagioclase (~25%), quartz (~30%),

454110*	454062*	454062*	454111*	454111*	454067*	40324a*	40329*	40160*	454027*	454029-A*	454029-E*	454029-A*
KI TP	KI N	KI N	KI QN	KI QN	KI QN	KS	KS	KS	ABC diorite	ABC syenite	ABC pillow	ABC syenite
ma	fr	fr	a	a	fr	mh	fb	k	mh	mh	g	g
Rim	Core	Rim	Core	Rim	Core							
7	3	7	9	7	6				18	6	15	12
49.36	50.54	49.82	50.69	50.33	49.30	47.61	46.77	45.78	45.81	47.31	52.40	52.16
1.43	0.82	1.00	0.95	1.21	1.05	0.55	1.23	1.79	2.02	1.18	0.07	0.09
3.39	1.67	1.60	0.74	0.60	1.50	5.99	3.54	2.11	6.86	5.06	0.16	0.51
17.91	21.68	23.23	25.35	26.94	22.27	15.11	32.13	29.92	19.23	20.11	28.42	27.18
1.86	2.11	2.14	2.07	2.18	1.70	0.27	0.97	1.73	0.33	1.62	1.72	3.49
9.58	8.17	6.82	4.24	3.12	7.40	14.19	2.61	2.66	10.38	10.26	12.86	12.30
2.80	4.93	4.71	0.99	0.89	6.08	11.97	8.15	5.42	10.73	9.71	0.98	1.21
7.86	5.99	5.99	8.49	8.32	4.94	0.95	2.81	5.46	1.53	1.22	0.05	0.07
1.42	1.15	1.15	1.38	1.42	1.06	0.71	0.95	1.21	0.66	0.47	0.01	0.00
95.62	97.05	96.47	94.91	95.02	95.31	97.35	99.16	96.08	97.56	96.95	96.66	97.01
4.31	4.23	4.07	1.91	2.03	2.29	7.41	6.24	3.58	6.22	11.58	0.00	0.00
14.03	17.87	19.57	23.62	25.11	20.21	8.44	26.52	26.70	13.64	9.69	28.42	27.18
96.05	97.48	96.87	95.10	95.22	95.54	98.09	99.78	96.44	98.18	98.11	96.66	97.01
7.525	7.710	7.721	8.080	8.080	7.726	6.946	7.286	7.433	6.825	7.016	8.014	7.972
0.475	0.290	0.279	0.000	0.000	0.274	1.030	0.650	0.404	1.175	0.885	0.000	0.028
8.000	8.000	8.000	8.080	8.080	8.000	7.976	7.936	7.837	8.000	7.902	8.014	8.000
0.135	0.010	0.014	0.140	0.114	0.003	0.000	0.000	0.000	0.029	0.000	0.029	0.063
0.164	0.094	0.117	0.114	0.146	0.124	0.060	0.144	0.219	0.227	0.132	0.008	0.010
0.495	0.486	0.473	0.230	0.245	0.269	0.814	0.731	0.437	0.698	1.292	0.000	0.000
2.176	1.858	1.577	1.007	0.745	1.728	3.087	0.606	0.644	2.305	2.269	2.932	2.802
1.790	2.279	2.538	3.149	3.373	2.651	1.030	3.454	3.625	1.699	1.202	2.030	2.124
0.240	0.272	0.280	0.280	0.297	0.226	0.010	0.064	0.075	0.042	0.104	0.000	0.000
5.000	5.000	5.000	4.920	4.920	5.000	5.000	5.000	5.000	5.000	5.000	5.000	5.000
0.000	0.000	0.000	0.000	0.000	0.000	0.000	0.000	0.000	0.000	0.000	1.603	1.351
0.000	0.000	0.000	0.000	0.000	0.000	0.024	0.064	0.163	0.000	0.098	0.222	0.452
0.459	0.806	0.784	0.169	0.154	1.022	1.876	1.364	0.944	1.716	1.549	0.160	0.197
1.541	1.194	1.216	1.831	1.846	0.978	0.100	0.573	0.893	0.284	0.353	0.014	0.000
2.000	2.000	2.000	2.000	2.000	2.000	2.000	2.000	2.000	2.000	2.000	2.000	2.000
0.788	0.583	0.587	0.795	0.746	0.524	0.169	0.278	0.829	0.160	0.000	0.001	0.021
0.277	0.223	0.228	0.281	0.291	0.212	0.132	0.189	0.251	0.126	0.089	0.001	0.001
1.065	0.806	0.815	1.076	1.037	0.736	0.302	0.468	1.080	0.286	0.089	0.002	0.021
16.065	15.806	15.815	16.076	16.037	15.736	15.278	15.404	15.917	15.286	14.990	15.016	15.021
48.7	40.2	34.4	23.0	17.1	37.2	62.6	12.7	13.7	49.0	47.6	44.7	44.6

partially chloritised biotite (~3%), FeTi-oxides (~2%) and accessory apatite and zircon.

5. Mineral chemistry

5.1. Pyroxene

Due to high Na-contents in many of the pyroxenes (Table 2) they are presented in the Na–Mg–(Fe^{2+}+Mn) triangular diagram (Fig. 3), rather than the conventional pyroxene quadrilateral. The aegirine augites of the Kangerlussuaq Intrusion lie on a trend from relatively magnesian ($Mg\#_{53–59}$) and Na-poor ($Ac_{5–6}$) in the foyaites to high Na- ($Ac_{12–47}$) and very low Mg-contents ($Mg\#_{0–30}$) in the pulaskites and nordmarkites. With the exception of the aegirine augite from Peak 2005 Syenite ($Mg\#_0$, Ac_{45}), which is very similar to those in the pulaskites and nordmarkites, all the pyroxenes of the satellite intrusions are Na-poor with large variations in Mg-contents ($Mg\#_{8–68}$).

5.2. Amphibole

In the Kangerlussuaq Intrusion, the (magnesio)-katophorites of the main pulaskites show a restricted compositional variation (Si=7.3–7.4 p.f.u.; $Mg\#_{38–57}$; Na+K=2.0–2.5 p.f.u.), whereas the sodic–calcic amphiboles of the transitional pulaskites extend to higher Si-contents (Si=7.32–7.76 p.f.u.; $Mg\#_{35–60}$; Na+K=1.7–2.6 p.f.u.) (Fig. 4 and Table 3). In comparison, the amphiboles of the nordmarkites extend towards lower Mg# (10–57) and even higher Si-contents (7.45–8.08 p.f.u.) at varying alkali contents (Na+K=1.50–2.90 p.f.u.). The amphiboles of the Kærven Syenite Complex (Holm and Prægel, 1988) differ markedly from those of the Kangerlussuaq Intrusion by extending towards much lower Si (6.82–7.48 p.f.u.) and Na+K (0.40–1.97 p.f.u.) contents at varying $Mg\#_{9–63}$ (Fig. 4). The compositional variation of amphiboles from the Peak 2005 Syenite (Si, 7.50–8.07 p.f.u.; $Mg\#_{27–75}$; Na+K, 1.87–2.76 p.f.u.) and the Augite Syenite (Si, 7.45–7.75 p.f.u.; $Mg\#_{19–40}$; Na+K, 1.59–1.98 p.f.u.) cover much of the variation in the Kangerlussuaq Intrusion and resemble the variation in the nordmarkites by becoming Si-, Na- and K-richer from core to rim with decreasing Mg# (Fig. 4). As in the older Kærven Syenite Complex, amphiboles from the younger satellite intrusions, the Astrophyllite Bay Complex (Si=6.80–8.01 p.f.u.; $Mg\#_{39–49}$; Na+K=0.02–0.69 p.f.u.) and Snout Series Syenite (Si=7.08–7.12 p.f.u.; $Mg\#_{43–57}$; Na+K=0.65–0.71 p.f.u.) are also distinct from those of the Kangerlussuaq Intrusion in containing alkali-poor amphiboles.

6. Whole-rock major element composition

The syenites as a whole show an overall decrease in total alkalis (Fig. 2), Al_2O_3 (Fig. 5a), and to some extent also CaO (Fig. 5b), with increasing silica. Excluding the foyaites, similar variations are found for MgO and FeO_{total} with increasing silica (Fig. 5c and d). The foyaites are chemically very distinct from the other syenites with high Al_2O_3 and total alkali contents at moderate SiO_2 (~55 wt.%). The pulaskites and nordmarkites also tend to form separate groups. The older and younger satellite intrusions have major element contents broadly similar to the pulaskites and nordmarkites.

7. Isotope data

7.1. Sr, Nd, Hf and Pb isotopes

Fig. 6 shows the variation of initial ε_{Nd} and ε_{Hf} against $^{87}Sr/^{86}Sr_i$. In the Kangerlussuaq Intrusion, $^{87}Sr/^{86}Sr_i$, ε_{Ndi} and ε_{Hfi} range from 0.7043 to 0.7061, 4.9 to 2.3, and 11.1 to 5.2, respectively, from the foyaites to the quartz nordmarkites (Riishuus et al., submitted for publication-b). The older satellite intrusions (Peak 2005 Syenite and Augite Syenite) overlap the Kangerlussuaq Intrusion with $^{87}Sr/^{86}Sr_i$=0.7047–0.7062, ε_{Ndi}=1.5–4.3 and ε_{Hfi}=2.5–8.4 (Fig. 6 and Table 4). Nd-, Hf- and Pb-isotope data are not available for the Kærven Syenite Complex but Sr-isotopes show considerable variation ($^{87}Sr/^{86}Sr_i$=0.7083–0.7364) (Holm, 1991). The younger satellite intrusions have less radiogenic ε_{Ndi} and ε_{Hfi} values than all the older intrusions and extend to much more radiogenic $^{87}Sr/^{86}Sr_i$ values. The Snout Series, Bagnæsset and Astrophyllite Bay syenites show restricted compositional variations in Nd and Hf isotopes (ε_{Ndi}=−2.4 to 0.3; ε_{Hfi}=−4.2 to 1.8) but large variations in $^{87}Sr/^{86}Sr_i$ (0.7079–0.7317). The Biotite Granite has unradiogenic $^{87}Sr/^{86}Sr_i$ (0.7055) and the least radiogenic ε_{Ndi} (−4.8) and ε_{Hfi} (−12.8) values of the KAC. Mafic rocks from the Astrophyllite Bay Complex define a narrow field of $^{87}Sr/^{86}Sr_i$=0.7074–0.7087, ε_{Ndi}=−4.6 to −3.1 and ε_{Hfi}=−11.4 to −8.9 (Riishuus et al., 2005).

The Pb-isotope variations are shown in Fig. 7. Alkali feldspars from the Kangerlussuaq Intrusion have radiogenic Pb-isotope compositions similar to the least crustally contaminated Lower Basalts (e.g., Hansen and

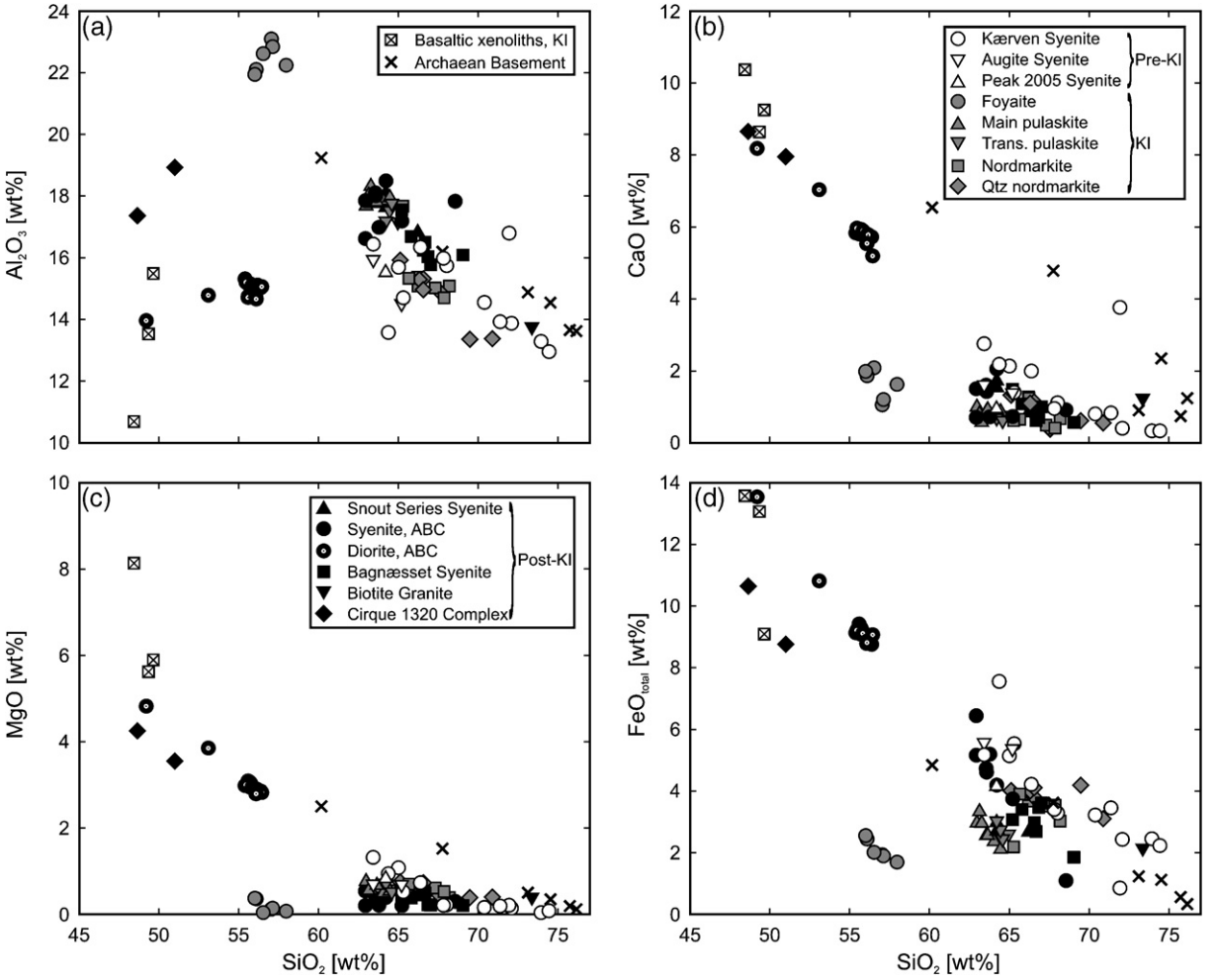

Fig. 5. Variation of selected whole-rock major oxides against silica in the Kangerlussuaq Alkaline Complex. The data are from Holm and Prægel (1988), Holm et al. (1991) (Kærven Syenite Complex), Riishuus et al. (submitted for publication-b) (Kangerlussuaq Intrusion), Riishuus et al. (2005) (Astrophyllite Bay Complex) and this study (Augite Syenite, Peak 2005 Syenite, Cirque 1320 Complex, Bagnæsset Syenite Complex, Snout Series Syenite and Biotite Granite).

Nielsen, 1999) and partly overlap with the virtually uncontaminated Plateau Basalts ($^{206}Pb/^{204}Pb > 17.7$) (e.g., Peate and Stecher, 2003). The Kangerlussuaq Intrusion spans $^{206}Pb/^{204}Pb_{meas}$=16.98–17.88 and $^{207}Pb/^{204}Pb_{meas}$=15.16–15.37 from the quartz nordmarkites to the radiogenic foyaites. $^{208}Pb/^{204}Pb_{meas}$ varies from 37.56–37.64 in the foyaites, through 37.71–37.91 in the pulaskites, to 37.46–37.95 in the nordmarkites. The older satellites have Pb-isotope compositions similar to the Kangerlussuaq Intrusion. The two Augite Syenite samples span $^{206}Pb/^{204}Pb_{meas}$=17.26–17.40, $^{207}Pb/^{204}Pb_{meas}$=15.20–15.23 and $^{208}Pb/^{204}Pb_{meas}$=38.15–38.19, while alkali feldspars of the Peak 2005 Syenite range from $^{206}Pb/^{204}Pb_{meas}$=17.45, $^{207}Pb/^{204}Pb_{meas}$=15.26 and $^{208}Pb/^{204}Pb_{meas}$=37.74 (phenocryst) to $^{206}Pb/^{204}Pb_{meas}$=17.81, $^{207}Pb/^{204}Pb_{meas}$=15.27 and $^{208}Pb/^{204}Pb_{meas}$=38.10 (matrix) (Fig. 7 and Table 4). As for Nd- and Hf-isotopes, the younger satellites define a distinct separate field of Pb isotope compositions that are much less radiogenic than the older intrusions. The Snout Series, Bagnæsset and Astrophyllite Bay syenites cover a field of $^{206}Pb/^{204}Pb_{meas}$=15.81–16.41, $^{207}Pb/^{204}Pb_{meas}$=14.96–15.07 and $^{208}Pb/^{204}Pb_{meas}$=36.53–37.09. The Biotite Granite has distinctly lower $^{208}Pb/^{204}Pb_{meas}$ (35.99). The mafic samples of the Astrophyllite Bay Complex span $^{206}Pb/^{204}Pb_{meas}$=15.64–15.91, $^{207}Pb/^{204}Pb_{meas}$=14.91–14.96 and $^{208}Pb/^{204}Pb_{meas}$=36.60–37.00. The KAC shows a wide range of $^{208}Pb/^{204}Pb_{meas}$ values at constant (low and high) $^{206}Pb/^{204}Pb_{meas}$ values.

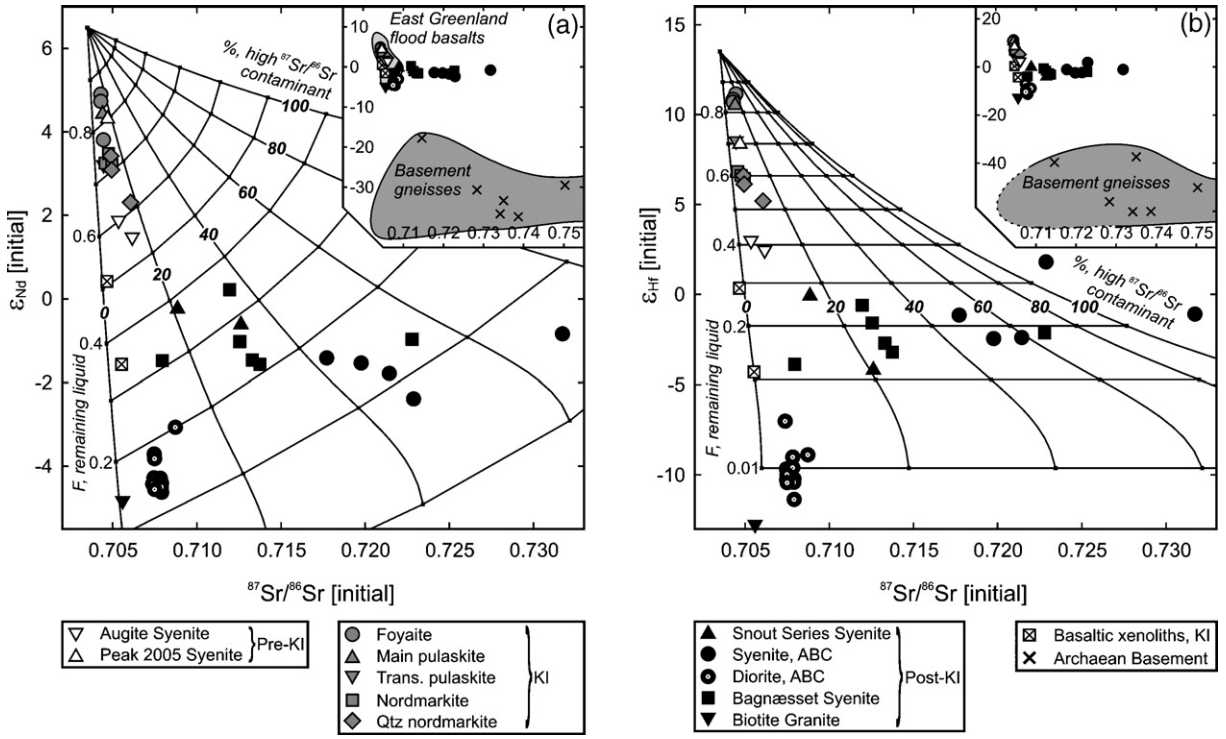

Fig. 6. Variations in (a) ε_{Ndi} and (b) ε_{Hfi} against $^{87}Sr/^{86}Sr_i$ of whole-rock samples from the Kangerlussuaq Alkaline Complex. The data are from this study and Riishuus et al. (2005, submitted for publication-b). Six modelled curves of assimilation and fractional crystallisation (DePaolo, 1981) between a magmatic end-member intermediate to the Plateau Basalts (Peate and Stecher, 2003; Andreasen et al., 2004) and the alkalic Prinsen af Wales Bjerge Formation basalts (Peate et al., 2003) ($^{87}Sr/^{86}Sr_i$=0.7035, Sr=300 ppm; ε_{Ndi}=6.5, Nd=30 ppm; ε_{Hfi}=13.5, Hf=5 ppm) and varying proportions of two different contaminants, granulite facies gneiss ($^{87}Sr/^{86}Sr_i$=0.706, Sr=500 ppm; ε_{Ndi}=−38, Nd=20 ppm; ε_{Hfi}=−65, Hf=2.5 ppm) and amphibolite facies gneiss ($^{87}Sr/^{86}Sr_i$=0.750, Sr=260 ppm; ε_{Ndi}=−36, Nd=5 ppm; ε_{Hfi}=−65, Hf=2.5 ppm) (based on Taylor et al., 1992; Riishuus et al., 2005, submitted for publication-b). The *r*-value (assimilation rate/crystallisation rate) is set to 0.3. D_{Sr}=0.20, D_{Nd}=0.28, and D_{Hf}=0.29 for F=1–0.9 (60% ol, 30% cpx, 10% trapped liquid); D_{Sr}=1.29, D_{Nd}=0.32 and D_{Hf}=0.38 for F=0.9–0.2 (60% plag, 30% cpx, 10% trapped liquid); D_{Sr}=1.78, D_{Nd}=0.40 and D_{Hf}=0.42 for F=0.2–0.01 (80% kspr, 10% cpx, 10% trapped liquid). Partition coefficients used in the interval F=1–0.2: Kd^{ol}_{Sr}=0.01 (Villemant, 1988), Kd^{ol}_{Nd}=0.0023 (Fujimaki et al., 1984), Kd^{ol}_{Hf}=0.04 (Villemant et al., 1981), Kd^{cpx}_{Sr}=0.3 (Shimizu, 1980), Kd^{cpx}_{Nd}=0.6 (Shimizu, 1980), Kd^{cpx}_{Hf}=0.56 (Fujimaki et al., 1984), Kd^{plag}_{Sr}=1.83 (Philpotts and Schnetzler, 1970), Kd^{plag}_{Nd}=0.069 (Schnetzler and Philpotts, 1970), Kd^{plag}_{Hf}=0.19 (Villemant, 1988). Partition coefficients used in the interval F=0.2–0.01: Kd^{kspr}_{Sr}=2 (Nagasawa, 1973), Kd^{kspr}_{Nd}=0.084 (Nagasawa, 1973), Kd^{kspr}_{Hf}=0.38 (Villemant, 1988), Kd^{cpx}_{Sr}=0.8 (Nagasawa, 1973), Kd^{cpx}_{Nd}=2.3 (Nagasawa, 1973), Kd^{cpx}_{Hf}=0.15 (Lemarchand et al., 1987). The inset in (a) shows regional variations of East Greenland flood basalts (Lower Basalts (Holm, 1988; Fram and Lesher, 1997; Hansen and Nielsen, 1999); Plateau Basalts (Peate et al., 2003; Peate and Stecher, 2003; Andreasen et al., 2004)) and basement gneisses (Taylor et al., 1992; Riishuus et al., 2005, submitted for publication-b).

7.2. Oxygen and hydrogen isotopes

The primary igneous minerals from the Kangerlussuaq Intrusion have $\delta^{18}O$ values from −2.4‰ to 6.0‰ (Fig. 8), and, as shown by Riishuus et al. (submitted for publication-a), the linear relationships of alkali feldspar (fsp) vs. pyroxene/amphibole mixture (px/amph) and alkali feldspar vs. quartz (qtz) are parallel to the equilibrium lines of constant per mil difference (Δ) indicating that the minerals crystallised in O-isotope equilibrium (Fig. 8). The Peak 2005 Syenite has $\delta^{18}O$ values of 3.2‰ (fsp phenocryst), 2.2‰ (fsp matrix) and 0.4‰ (px/amph) (Table 5). The Augite Syenite samples have $\delta^{18}O$ values of 3.8‰ (fsp phenocryst), 0.9‰ (px/amph), and −3.9‰ (fsp matrix) for 454076 and 5.8‰ (qtz), 4.1‰ (fsp), and 1.7‰ (px/amph) for 454077. The very negative $\delta^{18}O$ value of the matrix alkali feldspar from 454076 suggests that it interacted with an infiltrating, externally derived fluid. In spite of the limited number of samples, the observation that the other phases of both the Peak 2005 Syenite and Augite Syenite fall in the field of the Kangerlussuaq Intrusion (Fig. 8) indicates high-temperature O-isotope equilibrium. The Bagnæsset Syenite Complex forms a tight group with $\delta^{18}O$ values of 4.7–5.4‰ (fsp), 2.5–3.7‰ (px/amph) and 6.8‰ (qtz). The pyroxene/amphibole vs. alkali feldspar trend is parallel to the constant Δ equilibrium lines and inside the

Table 4
Major elements and Sr–Nd–Hf–Pb isotopes from the Kangerlussuaq Alkaline Complex, East Greenland

Sample whole rock	Intrusion	Sample location	SiO_2	TiO_2	Al_2O_3	Fe_2O_3	FeO	MnO	MgO	CaO	Na_2O	K_2O	P_2O_5	LOI	Total	(Na+K)/Al	$^{87}Sr/^{86}Sr$ initial	ε_{Nd} initial	ε_{Hf} initial	Sample	$^{206}Pb/^{204}Pb$ measured	$^{207}Pb/^{204}Pb$ measured	$^{208}Pb/^{204}Pb$ measured
454034	SS	13	66.10	0.64	16.79	0.96	1.81	0.13	0.50	0.83	5.97	5.99	0.11	0.13	99.83	1.06	0.71225	−0.5	−4.2	454034 undif	15.812	14.966	36.689
454045	SS	19	64.39	0.86	17.67	1.36	1.77	0.13	0.72	1.73	6.64	4.78	0.21	0.09	100.26	0.95							
454046	SS	19	63.86	0.74	18.00	1.39	1.44	0.12	0.54	1.52	6.78	4.87	0.19	0.19	99.45	0.95	0.70882	−0.2	−0.1	454046 undif	16.157	15.030	36.974
454070	BG	26	73.08	0.30	13.71	1.15	1.11	0.02	0.40	1.24	4.04	4.49	0.07	0.45	99.60	0.93	0.70554	−4.8	−12.8	454070 undif	15.907	14.993	35.993
454076	AS	30	64.89	0.92	14.44	2.25	3.32	0.23	0.69	1.38	6.71	4.55	0.15	0.13	99.52	1.15	0.70535	1.9	3.0	454076 undif	17.404	15.230	38.188
454077	AS	31	63.13	0.93	15.86	2.11	3.65	0.24	0.70	1.60	7.79	3.30	0.23	0.00	99.54	1.01	0.70616	1.5	2.5	454077 undif	17.259	15.199	38.147
454084	PS	33	64.04	1.06	15.48	2.26	2.10	0.26	0.83	0.94	7.46	5.06	0.26	0.37	99.75	1.19	0.70469	4.3	8.4	454084 phx	17.452	15.261	37.741
454107	CC	42	48.02	2.56	17.13	4.91	6.08	0.22	4.20	8.54	4.28	1.47	1.32	0.13	98.73	0.48				454084 mtx	17.806	15.275	38.097
454108	CC	42	50.51	2.05	18.75	4.21	4.89	0.17	3.52	7.87	4.64	1.61	0.84	0.32	99.07	0.48							
29403	BS	45	68.86	0.35	16.05	0.42	1.47	0.12	0.20	0.56	5.53	6.14	0.04	0.29	99.73	1.08	0.72226	−0.9	−2.1	29403 undif	16.038	14.998	36.708
29404	BS	45	66.04	0.46	15.84	1.20	2.35	0.23	0.22	0.70	5.83	5.88	0.04	−0.02	98.78	1.10	0.71179	−1.0	−1.6	29404 undif	16.275	15.049	36.976
40501	BS	47	65.20	0.55	16.54	1.85	1.70	0.14	0.37	1.07	5.84	5.75	0.07	0.20	99.10	1.04	0.71366	−1.5	−3.2	40501 undif	16.333	15.067	37.058
40568	BS	48	64.51	0.52	17.37	0.84	2.28	0.12	0.43	1.47	6.19	5.11	0.10	0.20	98.95	0.96	0.70791	−1.4	−3.9	40568 undif	16.171	15.029	36.903
40582	BS	49	66.31	0.66	16.41	0.67	2.07	0.12	0.48	0.61	6.24	5.77	0.10	−0.03	99.44	1.08	0.71195	0.3	−0.6	40582 undif	16.410	15.074	37.044
40583	BS	49	65.99	0.62	16.10	1.15	1.91	0.15	0.45	0.87	5.92	5.87	0.09	0.17	99.12	1.09							
40584	BS	49	66.56	0.46	15.65	1.06	2.63	0.19	0.21	1.00	5.74	5.76	0.04	0.14	99.29	1.09	0.71330	−1.4	−2.7	40584 undif	16.170	14.990	36.903
454089[a]	KI-F		55.35	0.54	21.69	1.76	0.93	0.19	0.37	1.96	9.34	6.62	0.10	0.84	98.85	1.08	0.70444	3.8	11.1	454089 undif	17.783	15.350	37.557
454048[a]	KI-MP		63.40	0.91	17.72	1.34	1.34	0.18	0.60	0.86	7.21	6.04	0.16	0.38	99.76	1.11	0.70440	4.4	10.5	454048 undif	17.686	15.331	37.708
454110[a]	KI-TP		64.06	0.55	17.62	1.35	1.21	0.13	0.52	0.62	7.71	5.30	0.11	0.39	99.18	1.09	0.70447	3.2	8.5	454110 undif	17.666	15.292	37.907
454062[a]	KI-N		65.56	0.78	15.22	1.91	1.92	0.22	0.66	1.26	6.74	4.61	0.16	0.23	99.02	1.10	0.70476	3.5	6.6	454062 undif	17.206	15.212	37.691
454111[a]	KI-QN		69.25	0.25	13.31	2.63	1.81	0.23	0.39	0.61	6.19	4.94	0.07	0.46	99.68	1.23	0.70489	3.4	6.6	454111 undif	17.254	15.208	37.948
454067[a]	KI-QN		66.29	0.80	15.26	1.56	2.38	0.23	0.65	1.07	6.75	4.43	0.18	0.08	99.59	1.08	0.70607	2.3	5.2	454067 undif	16.977	15.160	37.685
40160[a]	KS		71.20	0.27	13.70	1.59	0.97	0.080	0.14	0.40	5.39	5.01	0.03		98.78	1.13							
3[a]	KS		65.07	0.78	14.65	1.92	3.78	0.18	0.52	1.40	5.58	4.97	0.80	0.11	99.65	1.07							
454026[a]	ABC-diorite		52.67	2.68	14.67	2.89	8.12	0.19	3.82	6.98	4.28	2.01	0.91	0.24	99.22	0.62	0.70745	−4.3	−9.7	454026 wr	15.907	14.964	37.003
P5-A[a]	ABC-pillow		54.92	2.08	15.18	2.41	6.88	0.21	2.95	5.78	5.95	1.82	0.97	0.08	99.15	0.74	0.70791	−4.6	−11.4	P5-A wr	15.786	14.946	36.877
P5-L[a]	ABC-syenite		63.32	0.76	17.94	2.24	2.58	0.14	0.40	1.41	6.78	3.96	0.06	0.08	99.60	0.88	0.71975	−1.5	−2.5	P5-L wr	15.818	14.964	36.525

SS, Snout Series Syenite; BG, Biotite Granite; AS, Augite Syenite; PS, Peak 2005 Syenite; CC, Cirque 1320 Complex; BS, Bagnæsset Syenite; KI, Kangerlussuaq Intrusion; F, foyaite; MP, main pulaskite; TP, transitional pulaskite; N, nordmarkite; QN, quartz nordmarkite; ABC, Astrophyllite Bay Complex; KS, Kærven Syenite. Sample location, see Fig. 1b; LOI, loss on ignition; undif, undifferentiated alkali feldspar (one or several populations); phx, alkali feldspar phenocryst; mtx, matrix alkali feldspar; wr, whole rock.

[a] Representative samples compiled from published and unpublished data: KI (Riishuus et al., submitted for publication-b), KS (Holm and Prægel, 1988; Holm et al., 1991) and ABC (Riishuus et al., 2005).

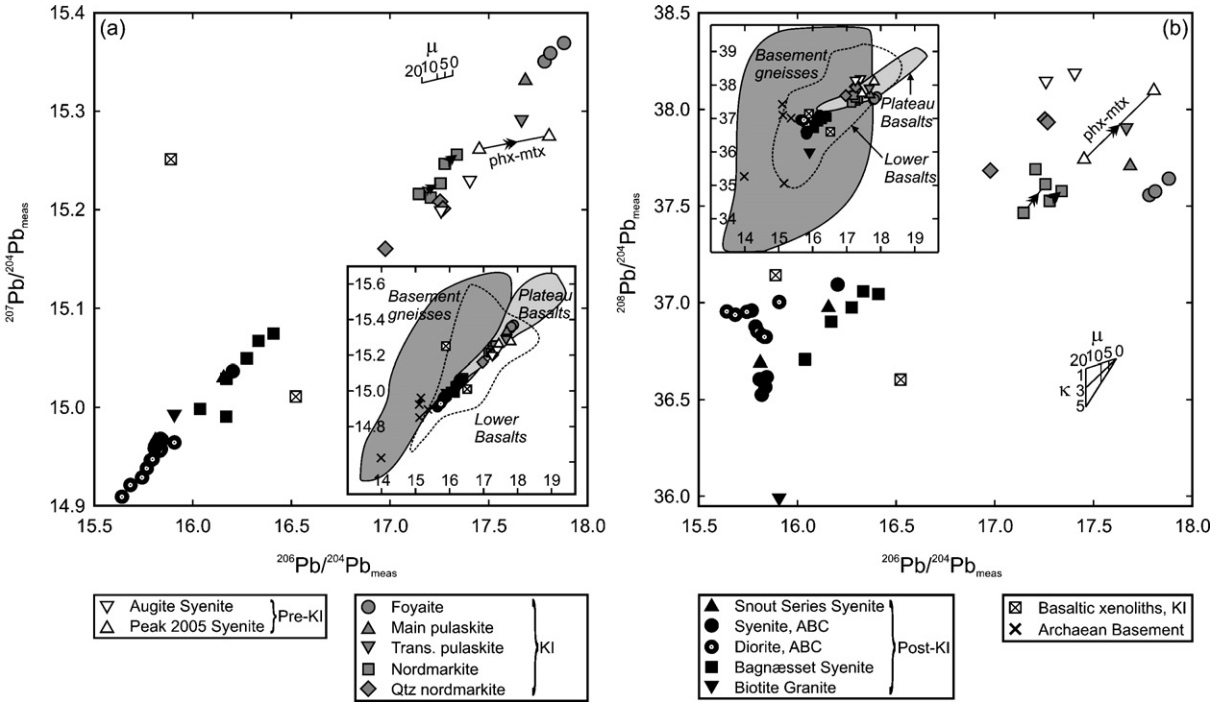

Fig. 7. Variations in (a) $^{207}Pb/^{204}Pb_{meas}$ and (b) $^{208}Pb/^{204}Pb_{meas}$ against $^{206}Pb/^{204}Pb_{meas}$ of alkali feldspar and whole-rock samples from the Kangerlussuaq Alkaline Complex (Riishuus et al., 2005, submitted for publication-b; this study). Tie-lines with arrows indicate compositional change from phenocryst to matrix of co-existing alkali feldspar populations. Vectors show the effects of age correction to 50 Ma for different μ ($^{238}U/^{204}Pb$) and κ ($^{232}Th/^{238}U$) values. The μ and κ values for the Kangerlussuaq Intrusion, where U, Th and Pb concentrations are available, range over 2–16 and 0.5–2.7 (one sample, 454079, is 28.5 and 5.4) with averages of 8 and 1.4, respectively, which is far less than the variation between samples. Coexisting alkali feldspar phenocryst and matrix both have μ values of 11–12 and κ values of 0.5–0.7, so the isotopic variation between them appears to be a primary magmatic feature rather than related to age correction. The insets in (a) and (b) show the regional variations of East Greenland Lower Basalts (Holm, 1988; Fram and Lesher, 1997; Hansen and Nielsen, 1999), Plateau Basalts (Peate et al., 2003; Peate and Stecher, 2003; Andreasen et al., 2004) and basement gneisses (Leeman et al., 1976; Taylor et al., 1992; Riishuus et al., 2005, submitted for publication-b).

field of the Kangerlussuaq Intrusion (Fig. 8). Minerals of the Bagnæsset Syenite Complex must therefore also have crystallised in O-isotope equilibrium. The Astrophyllite Bay Complex samples have $\delta^{18}O$ values of 6.8–6.9‰ (plagioclase and fsp) and 5.1‰ (px/amph), and the single sample in Fig. 8, located on the extension of the Kangerlussuaq Intrusion pyroxene/amphibole vs. alkali feldspar trend, shows no sign of alteration. The Biotite Granite ($\delta^{18}O=7.0$‰, fsp; $\delta^{18}O=6.8$‰, qtz) and the Snout Series Syenite ($\delta^{18}O=5.8$–6.6‰, fsp; $\delta^{18}O=0.7$–2.1‰, px/amph) have larger $\Delta_{\text{alkali feldspar-qtz}}$ and $\Delta_{\text{alkali feldspar-px/amph}}$ than the rest of the KAC, and although the number of samples is limited, there is no evidence of O-isotope disequilibrium.

As the bulk of the $\delta^{18}O$ data indicate O-isotope equilibrium crystallisation at magmatic conditions, we estimate $\delta^{18}O$ values of the original magmas (Table 5) using the mineral-melt fractionation factors ($\Delta_{\text{mineral-magma}}$) given by Harris (1995): $\Delta_{\text{quartz-magma}}=1$‰ for fine-grained plutonic rocks (the Biotite Granite) and 2‰ for coarse-grained plutonic rocks (the rest), $\Delta_{\text{feldspar-magma}}=0.2$‰ and $\Delta_{\text{pyroxene/amphibole-magma}}=-0.8$‰. The $\delta^{18}O$ magma values of the Kangerlussuaq Intrusion vary from very low in the nordmarkites (−1‰ to 4‰) to 5.8‰ in the foyaites (Riishuus et al., submitted for publication-a). The Peak 2005 Syenite $\delta^{18}O$ magma values span 1.2–3.0‰, whereas the Augite Syenite values span 1.7–3.9‰. The magma $\delta^{18}O$ values of the Bagnæsset Syenite Complex are slightly higher than the older satellite intrusions with 3.3–5.2‰, whereas those of the Snout Series Syenite are 1.5–6.4‰. The highest magma $\delta^{18}O$ values occur in the Astrophyllite Bay Complex (5.1–6.9‰) and the Biotite Granite (6.2–6.8‰).

The hydrogen isotope compositions of amphiboles from the Kangerlussuaq Intrusion increase from very negative δD values (−157‰ to −143‰) throughout the nordmarkites to values of −113‰ to −86‰ in the pulaskites (Riishuus et al., submitted for publication-a). The δD values of the satellite intrusions vary from −173‰

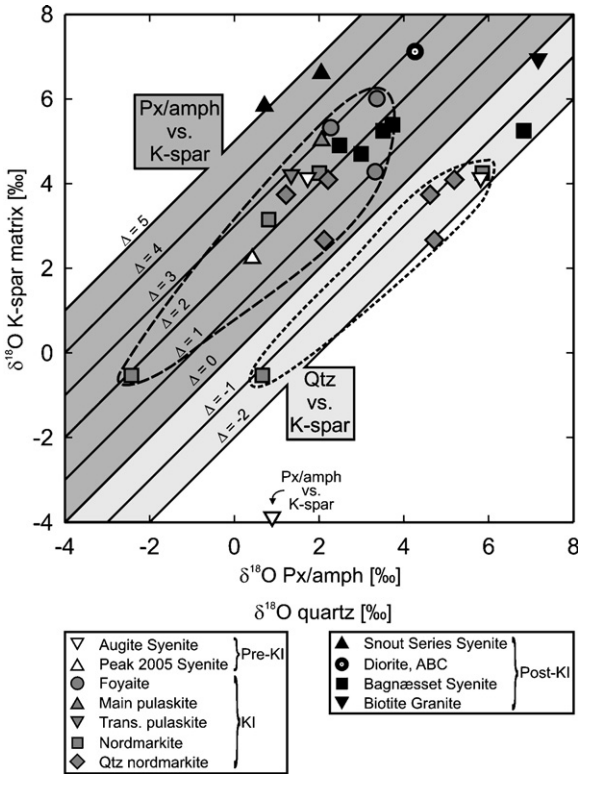

Fig. 8. $\delta^{18}O$ vs. $\delta^{18}O$ of coexisting mineral phases from the Kangerlussuaq Alkaline Complex (Riishuus et al., submitted for publication-a; this study). Oxygen isotope equilibrium lines for Δ mineral Y-mineral X of −2, −1, 0, 1, 2, 3, 4 and 5 are shown. Mineral pairs of alkali feldspar and pyroxene/amphibole are located in the dark gray field, whereas alkali feldspar–quartz pairings are located in the light gray field.

to −103‰ (Augite Syenite), over −141‰ (Peak 2005 Syenite) and −154‰ to −111‰ (Snout Series Syenite), to −105‰ (Astrophyllite Bay Complex, diorite) (Table 5).

8. Discussion

8.1. Parental magmas and source

The KAC samples extend to very unradiogenic $^{206}Pb/^{204}Pb$ compositions (Fig. 7) suggestive of a significant crustal component. However, the less contaminated intrusions of the complex, the Kangerlussuaq Intrusion, Augite Syenite and Peak 2005 Syenite, have more radiogenic $^{206}Pb/^{204}Pb$ compositions within the field of the essentially uncontaminated plateau basalts and thus require the strong influence of a mantle component.

Mafic alkaline dykes of alkali olivine basaltic, basanitic and trachybasaltic affinities are sparse relative to the felsic alkaline intrusions but do occur throughout the Kangerlussuaq district (Wager, 1947; Vincent, 1953; Brooks and Platt, 1975; Nielsen, 1978; Brooks and Nielsen, 1982; Nielsen, 1987; Riishuus et al., submitted for publication-b). These dykes were emplaced in several generations and both pre- and post-date the felsic intrusions. Evidence for production of under-saturated basic magma also comes from the alkaline lavas of the Prinsen af Wales Bjerge Formation (Brown et al., 1996; Hansen et al., 2002; Peate et al., 2003) and ultramafic cumulates of the large Gardiner complex (Nielsen, 1980, 1981). The presence of kaersutite gabbroic inclusions found in alkali basaltic to basanitic dykes cutting the KAC (Brooks and Platt, 1975) and a large, positive aeromagnetic anomaly associated with the KAC (Verhoef et al., 1996; Riishuus et al., submitted for publication-b) are further indications that primitive alkaline magmas were present in the area. In comparison, phonolites are very rare in this area and are only found as erratic blocks (Brooks and Rucklidge, 1974). On these grounds, we believe that the most likely parental magma (s) for the syenites were silica under-saturated and had basanitic to alkali basaltic compositions. Subsequent crustal contamination drove differentiated melts to silica-oversaturated compositions and gave rise to quartz-bearing syenites. We speculate that the large, mafic body beneath the KAC, inferred from geophysical data, may represent the crystalline products of several chambers that were originally stratified from alkali basalt/basanite to phonolite/trachyte and connected, through plumbing systems, with the large volumes of overlying syenite.

Mafic to ultramafic alkaline rocks from East Greenland related to the North Atlantic Igneous Province are suggested to originate from partial melting of (i) an enriched part within the proto-Icelandic plume upwelling under a thick lithospheric cap (Bernstein et al., 2000, 2001; Peate et al., 2003) and (ii) metasomatised shallow mantle that became enriched in LREE by volatiles and crystallisation of incipient melt ($\ll 1\%$) generated from the plume below (Storey et al., 2004). The syenites from the KAC are generally coarse-grained and too evolved and contaminated to carry information on potential mantle source(s). Fractionation models for basanite–phonolite suites suggest that phonolites represent 13–25% residuals of the parental basanites (Kyle, 1981; le Roex et al., 1990; Ablay et al., 1998). The Kangerlussuaq Intrusion has an estimated volume of ~4000 km^3 (Riishuus et al., submitted for publication-b), and the underlying mafic parent should therefore have a volume of ~20,000 km^3. The resultant supply rate would be 0.1 km^3/year, assuming a magmatic lifetime of ~200 k.y. for emplacement of the Kangerlussuaq Intrusion. Eldholm and Grue (1994) estimated the mean eruption

Table 5
Oxygen and hydrogen isotope compositions of minerals and calculated $\delta^{18}O$ magma values from the Kangerlussuaq Alkaline Complex

Sample	Intrusion	$\delta_{k\text{-spar, phx}}$	$\delta_{k\text{-spar, mtx}}$	δ_{plag}	δ_{quartz}	$\delta_{px/amph}$	δD_{amph}	δ_{magma} (k-spar, phx)	δ_{magma} (k-spar, mtx)	δ_{magma} (plag)	δ_{magma} (quartz)	δ_{magma} (px/amph)
454026	ABC-diorite			7			−105			6.8		
P5-A	ABC-pillow			7.1		4.3				6.9		5.1
P5-L	ABC-syenite		7.0						6.8			
454034	SS		5.8			0.7	−154		5.6			1.5
454046	SS		6.6			2.0	−111		6.4			2.8
454070	BG		7.0		7.2				6.8		6.2	
454076	AS	3.8	−3.9			0.9	−103	3.6	−4.1			1.7
454077	AS		4.1		5.8	1.7	−173		3.9		3.8	2.5
454084	PS	3.2	2.2			0.4	−141	3.0	2.0			1.2
29403	BS		5.3		6.8	3.5			5.1		4.8	4.3
29404	BS		4.7			3.0			4.5			3.8
40501	BS		5.4			3.7			5.2			4.5
40584	BS		4.9			2.5			4.7			3.3
454089[a]	KI-F		6.0			3.4[p]			5.8			4.2[p]
454048[a]	KI-MP		5.0			2.1	−113		4.8			2.9
454110[a]	KI-TP		4.2			1.3	−86 (8)		4.0			2.1
454096[a]	KI-N	−0.4	−0.5		0.7	−2.4	−147 (8)	−0.6	−0.7		−1.3	−1.6
454062[a]	KI-N	4.6	4.2		5.8	2.0	−157	4.4	4.0		3.8	2.8
454111[a]	KI-QN	3.9	4.1		5.2	2.2	−157 (2)	3.7	3.9		3.2	3.0
454067[a]	KI-QN	4.3	3.7		4.6	1.2	−143 (3)	4.1	3.5		2.6	2.0

ABC, Astrophyllite Bay Complex; SS, Snout Series Syenite; BG, Biotite Granite; AS, Augite Syenite; PS, Peak 2005 Syenite; BS, Bagnæsset Syenite; KI, Kangerlussuaq Intrusion; F, foyaite; MP, main pulaskite; TP, transitional pulaskite; N, nordmarkite; QN, quartz nordmarkite; KS, Kærven Syenite; phx, phenocryst; mtx, matrix. Figure in parenthesis, deviation from mean where duplicate analyses were performed. Mixed pyroxene/amphibole analyses marked p are only pyroxene analyses. The following values of $\Delta_{mineral\text{-}magma}$ have been applied to estimate $\delta^{18}O$ magma values: $\Delta_{quartz\text{-}magma}=1‰$ for fine-grained plutonic rocks, $\Delta_{quartz\text{-}magma}=2‰$ for coarse-grained plutonic rocks, $\Delta_{feldspar\text{-}magma}=0.2‰$ and $\Delta_{pyroxene/amphibole\text{-}magma}=-0.8‰$.
[a] Representative samples compiled from Riishuus et al. (submitted for publication-a).

rate of flood basalts belonging to the North Atlantic Igneous Province as ~0.6 km^3/year. The production rate estimates are very uncertain but serve to illustrate that huge volumes of source material underwent partial melting to produce large volumes of alkaline, basic magma in a relatively short period, which eventually differentiated in magma chambers to produce the syenites in the Kangerlussuaq area. This may indicate a source within the plume during passage of the East Greenland margin over its stem at ~50 Ma (Tegner et al., 1998a). However, a source outside the plume cannot be excluded.

8.2. Temporal evolution of the Kangerlussuaq Alkaline Complex

A number of chemical and isotopic parameters vary systematically with time (Fig. 9). The intrusions display a general decrease in whole-rock SiO_2-content and increase in whole-rock (Na+K)/Al, amphibole Na+K pf.u., ε_{Hfi} (and ε_{Ndi}) and $^{206}Pb/^{204}Pb_{meas}$ values from the early Kærven Syenite Complex through the foyaites of the Kangerlussuaq Intrusion. These trends do not continue through the younger satellite intrusions, which display a return to higher silica-contents and a decrease in all other parameters relative to the foyaites (Fig. 9).

The ε_{Ndi}, ε_{Hfi} and $^{206}Pb/^{204}Pb_{meas}$ values of the younger satellite intrusions are lower than any of the older intrusions and suggest greater amounts of crustal contamination (Figs. 6 and 7). Assuming a common magmatic end-member, modelled assimilation-fractional crystallisation curves (Fig. 6) suggest that the Sr–Nd–Hf isotopic signature of the younger satellites could be produced after 60–90% crystallisation, whereas the isotopic signatures of the older satellites and the Kangerlussuaq Intrusion are reached after only 20–60% and 15–45% crystallisation, respectively. The precursor magma to the Kangerlussuaq Intrusion syenites probably differentiated in a chamber that was less open to assimilation than those of the younger satellites. There is only Sr-isotope data that are available from the Kærven Syenite Complex ($^{87}Sr/^{86}Sr_i$= 0.7083–0.7364; Holm, 1991), and hence, the degree of crustal contamination in this complex is poorly constrained. We explain the tendency towards higher silica contents and lower whole-rock (Na+K)/Al and amphibole Na+K p.f.u. of especially the younger satellites, but also the older Kærven Syenite Complex,

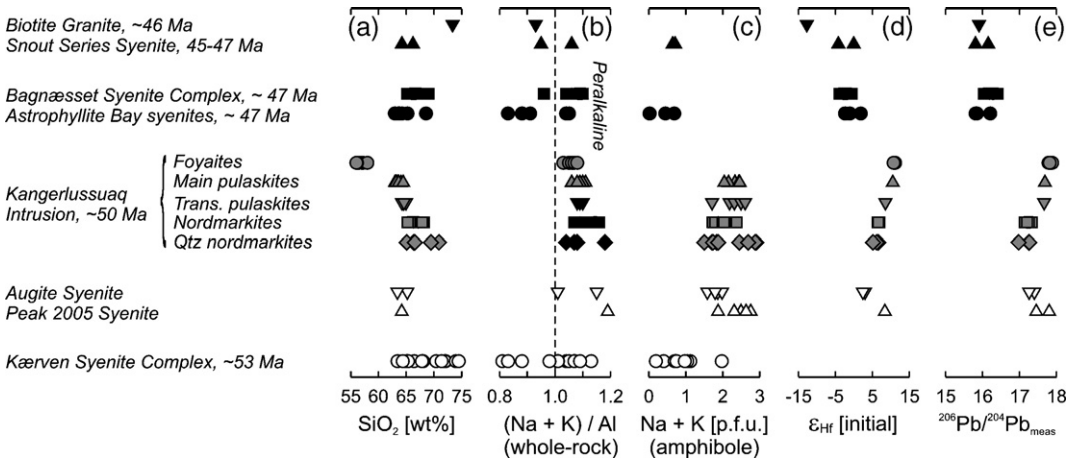

Fig. 9. Chronological compilation of the intrusions of the Kangerlussuaq Alkaline Complex against (a) whole-rock SiO_2, (b) whole-rock (Na+K)/Al, (c) amphibole Na+K content, (d) ε_{Hfi} and (e) $^{208}Pb/^{204}Pb_{meas}$. The ages are from Pankhurst et al. (1976) (Kangerlussuaq Intrusion), Riishuus et al. (2005) (Astrophyllite Bay Complex/Bagnæsset Syenite Complex) and (Tegner et al., submitted for publication) (Kærven Syenite Complex, Snout Series Syenite and Biotite Granite). The data are from Holm and Prægel (1988), Holm et al. (1991) (Kærven Syenite Complex), Riishuus et al. (submitted for publication-b) (Kangerlussuaq Intrusion), Riishuus et al. (2005) (Astrophyllite Bay Complex) and this study (Augite Syenite, Peak 2005 Syenite, Cirque 1320 Complex, Bagnæsset Syenite Complex, Snout Series Syenite and Biotite Granite).

by assimilation of less alkaline, silica-rich crustal material. In essence, the magmas of the KAC appear to have evolved from a less alkaline, silica-rich and crustally contaminated stage through a more alkaline, silica-poor and less contaminated stage, before returning to less alkaline, silica-rich and strongly crustally contaminated magmatism. The mantle-to-crust ratio reached a maximum in the foyaites, which crystallised from phonolitic magma that experienced only limited crustal contamination.

The geographical location and volume of the different intrusions of the KAC can be related to the degree of silica saturation, alkalinity and amount of crustal contamination (Table 1, Figs. 1 and 9). This relationship can best be explained as a consequence of changing magma supply rates and the re-establishment of plumbing systems due to relocation of the centre of magmatic activity. The magmatism started in the north-east with formation of the Kærven Gabbro and the Kærven Syenite Complex, but also with pre-Kangerlussuaq Intrusion activity in the western part, the Augite Syenite and the Peak 2005 Syenite (Fig. 1). Establishment of an early plumbing system in the Kærven area resulted in production of crustally contaminated quartz syenites and alkali feldspar granites. The subsequent syenitic units from Kærven become younger towards the west (Holm and Prægel, 1988; Holm et al., 1991), indicating that the centre of activity gradually moved southwest away from the fjord (Fig. 1). The magma supply rate increased significantly around 50 Ma and the activity became more focused when a new and larger plumbing system developed under the Kangerlussuaq Intrusion. The syenitic cumulates that formed in the magma chamber of the Kangerlussuaq Intrusion became increasingly alkaline, silica-poor and less contaminated, as the plumbing system became increasingly armoured against country rock assimilation and more and more uncontaminated magma was tapped from the underlying master chamber (Riishuus et al., submitted for publicationn-b). The effect of frequent magmatic recharge is visible in individual samples, as matrix alkali feldspars are less contaminated than coexisting phenocrysts (Fig. 7). Magmatism in this area did not cease until the phonolitic magma had been emplaced. The centre of activity then moved southeast where new, less productive, plumbing systems were established around Amdrup Fjord at 45–47 Ma (Fig. 1). This renewed phase gave rise to less alkaline, silica-rich and strongly contaminated syenites and granites of the Bagnæsset Syenite Complex, Snout Series Syenite and Biotite Granite. We speculate that the southeast displacement of the focus of the magmatism could be related to the northwest movement of Greenland relative to the proto-Icelandic mantle plume (Tegner et al., 1998a).

8.3. Role of magma supply rates

8.3.1. Production-dependent ponding and contamination of magmas

Crustal contamination of East Greenland offshore and onshore continental break-up related basalts (Fitton et al., 1998; Hansen and Nielsen, 1999; Andreasen et al., 2004)

and the Astrophyllite Bay Complex (Riishuus et al., 2005) have shown that two types of gneissic contaminants, granulite-facies (unradiogenic Sr) and amphibolite-facies (radiogenic Sr), can be recognised (Fig. 6). Although the detailed distribution of these two principal types of gneisses in East Greenland is complicated, it appears, on the basis of pressure estimates of magma ponding levels and contamination of the Astrophyllite Bay Complex, that an overall simple, stable crustal structure exists in the Kangerlussuaq area with granulite facies gneiss dominant in the lower crust and amphibolite facies gneiss in the upper crust (Riishuus et al., 2005). The $^{87}Sr/^{86}Sr_i$ values of the younger Snout Series, Bagnæsset and Astrophyllite Bay (Fig. 6) and the older Kærven (Holm, 1991) syenites extend to very radiogenic compositions. This suggests that their precursor magmas spent more time ponding in the upper crust, with ensuing contamination, than those of the Kangerlussuaq Intrusion, Augite Syenite and Peak 2005 Syenite.

Early flood basalts at ODP leg 152, southeast Greenland, were contaminated by granulite while later lavas by amphibolite facies gneisses (Fitton et al., 1998). The opposite is, however, observed in the Lower Basalts of central East Greenland (Hansen and Nielsen, 1999). In both rifting environments, it is the evolved lava sequences, extruded during low magma supply rates, which show contamination by amphibolite facies gneisses. This led Hansen and Nielsen (1999) to suggest that the magma supply rate governs the ponding level in the crust. At low magma supply rates shallow ponding with contamination of relatively fusible amphibolitic gneiss with hydrous silicates is favoured. Stabilisation of high rates should allow deep crustal ponding and partial melting of less refractory, dry, granulitic gneiss. Following this tenet, we suggest that the KAC evolved from low-volume intrusions with $^{87}Sr/^{86}Sr_i$ extending to high values, through high volume with low $^{87}Sr/^{86}Sr_i$, before returning to low volume with increasing $^{87}Sr/^{86}Sr_i$ (Fig. 10).

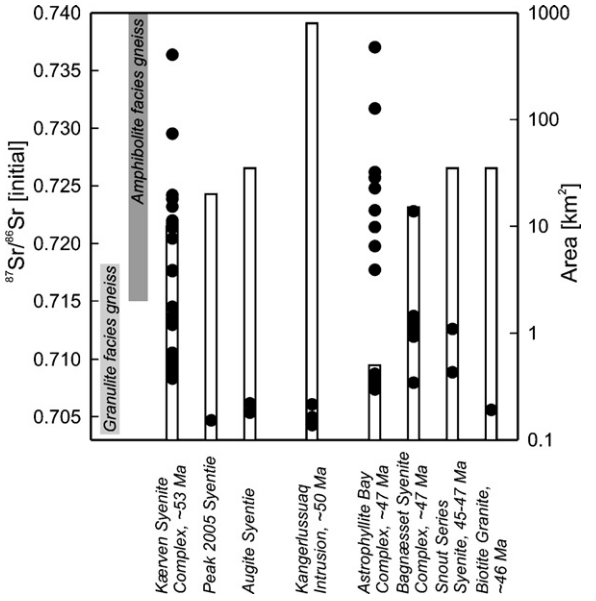

Fig. 10. Correlation of whole-rock $^{87}Sr/^{86}Sr_i$ (black points) with area (vertical white bars) of intrusions belonging to the Kangerlussuaq Alkaline Complex. Temporal variations in (i) $^{87}Sr/^{86}Sr_i$ are assumed to represent changes in magma ponding levels, where low $^{87}Sr/^{86}Sr_i$ values are related to contamination by lower crustal granulite facies gneiss and high $^{87}Sr/^{86}Sr_i$ values by upper crustal amphibolite facies gneiss, and (ii) area are assumed to represent changes in magma productivity. The Sr isotope data for the Kangerlussuaq Alkaline Complex are from Holm (1991), Riishuus et al. (2005, submitted for publication-b) and this study, and those of the East Greenland gneisses are from Taylor et al. (1992) (granulite gneisses from Ammassalik to Kangerlussuaq, $^{87}Sr/^{86}Sr_i = 0.703–0.718$) and Blichert-Toft et al. (1992), Taylor et al. (1992) and Riishuus et al. (2005, submitted for publication-b) (amphibolite gneisses in the Kangerlussuaq area, $^{87}Sr/^{86}Sr_i = 0.715–0.783$).

8.3.2. Role of emplacement level on magma $\delta^{18}O$ compositions

Riishuus et al. (submitted for publication-a) showed that the nordmarkites sensu lato of the Kangerlussuaq Intrusion crystallised from quartz trachyte magma depleted in ^{18}O ($\delta^{18}O = -1‰$ to $+4‰$) relative to the mantle (Fig. 11). The driving process for production of the low-$\delta^{18}O$ magma was interpreted as the assimilation of ^{18}O-depleted water released by the dehydration of basaltic xenoliths that had been hydrothermally altered by meteoric water prior to incorporation in the magma chamber (Riishuus et al., submitted for publication-a). Ultimately, this was caused by very shallow emplacement of the magma, which stoped into the lava pile (Fig. 1c). Only by repeated recharge with mantle-derived magma, and cessation of the supply of basalt xenoliths due to roof-downward crystallisation and/or stabilization of the roof, did the $\delta^{18}O$ value of the residual magma finally reach a mantle signature when the final foyaites crystallised (Fig. 11).

The older Augite and Peak 2005 syenites are also characterised by low $\delta^{18}O$ magma values similar to the nordmarkites of the Kangerlussuaq Intrusion (Fig. 11). The Augite Syenite has a very large basaltic xenolith/syenite ratio and, although no basaltic xenoliths have been observed in the Peak 2005 Syenite, a similar process is suggested for these intrusions to explain their low $\delta^{18}O$ magma values. The calculated $\delta^{18}O$ magma values for the Bagnæsset Syenite Complex are only slightly lower than expected for a mantle-derived magma (Fig. 11). The Bagnæsset Syenite Complex and the

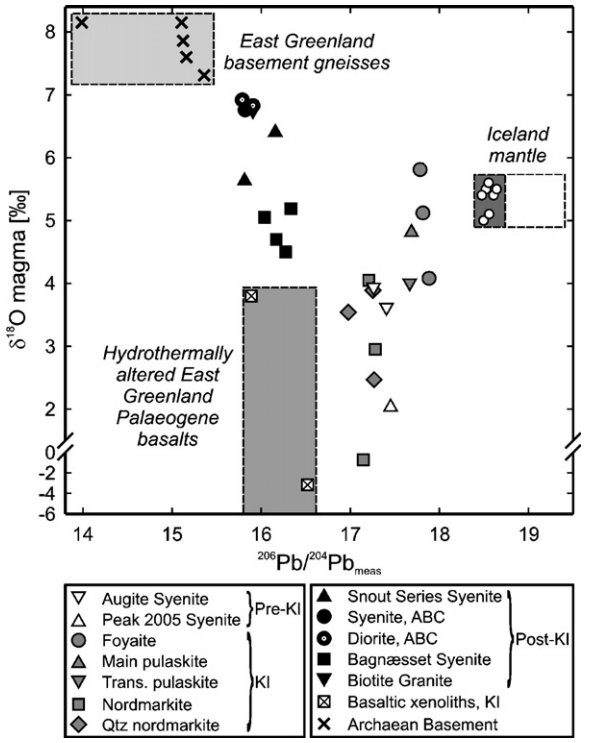

Fig. 11. Calculated $\delta^{18}O$ magma values plotted against $^{206}Pb/^{204}Pb_{meas}$ compositions of the Kangerlussuaq Alkaline Complex (Riishuus et al., 2005, submitted for publication-a,b; this study). Fields of East Greenland gneisses (Riishuus et al., 2005, submitted for publication-a,b; this study), hydrothermally altered basalts (Brandriss et al., 1996; Riishuus et al., submitted for publication-a,b) and Iceland mantle (Prestvik et al., 2001) are shown.

Snout Series Syenite host fewer basaltic xenoliths than the Kangerlussuaq Intrusion but are much more contaminated by basement. The $\delta^{18}O$ magma values of these intrusions can best be explained by the addition of high $\delta^{18}O$ material by greater assimilation of basement and less basalt dehydration compared to the Augite and Peak 2005 syenites. The Astrophyllite Bay Complex and the Biotite Granite have $\delta^{18}O$ magma values that are higher than expected for a mantle-derived magma and no basaltic xenoliths have been observed. As suggested by Riishuus et al. (2005) for the Astrophyllite Bay Complex, these intrusions appear to have been emplaced below the unconformity between the gneissic basement and the Palaeogene plateau basalts, and their $\delta^{18}O$ magma values have consequently only been modified by contamination with gneiss.

The δD of amphiboles (−173‰ to −86‰) from the KAC extend to values far below that of mantle-derived magmas (−80‰, Kyser (1986)). The variation within the Kangerlussuaq Intrusion (−157‰ to −86‰) can be explained by several processes: (i) addition of deuterium-depleted water from dehydration of basaltic xenoliths, (ii) magma recharge, (iii) magma degassing, and (iv) composition-dependent amphibole-melt D/H fractionation (Riishuus et al., submitted for publication-a). The δD values of amphiboles from the satellite intrusions (−173‰ to −103‰) can also be explained by one or several of these processes. Some overprint of the δD values by subsolidus hydrogen isotope exchange cannot be excluded.

It emerges that the final emplacement levels of the evolved magmas are related to the degree of crustal contamination. The least contaminated magmas stoped into the basalt pile, whereas the most crustally contaminated magmas never came in contact with the flood basalts. The correlation of emplacement level and degree of contamination could be due to a combination of two factors: (i) a higher magma production rate which led to a shallower level of neutral buoyancy in the crust because of magmatic over-pressure, and (ii) increased assimilation and fractional crystallisation leading to higher silica-content and viscosity that hindered upward migration.

9. Conclusions

(1) The Kangerlussuaq Alkaline Complex hosts a variety of rocks with alkaline to peralkaline affinity encompassing alkali gabbro/diorite, syenite, granite and nepheline syenite, and it is dominated by felsic rocks at the present exposure level. The preferred origin for the parental magmas involves low degrees of melting of a mantle source giving rise to basanitic to alkaline basaltic compositions. This is supported by kaersutite gabbroic xenoliths in dykes and geophysical evidence indicating large volumes of mafic material below the complex.

(2) The intrusions of the Kangerlussuaq Alkaline Complex are explained as products of varying amounts of assimilation and fractional crystallisation of primitive silica under-saturated alkaline magmas. Contamination of the magmas was controlled by supply rates so that ponding in lower crustal granulite facies gneisses took place at times of high supply rates, whereas ponding in upper crustal amphibolite-facies gneisses dominated during low supply rates.

(3) The degree of silica saturation, alkalinity and crustal contamination may be linked with the temporal evolution of the Kangerlussuaq Alkaline Complex. Establishment of the earliest plumbing system belonging to the Kærven Syenite Complex resulted in the production of crustally contaminated silica-rich syenites and

granites. The magmatism became increasingly more alkaline, silica-poor and less contaminated when the centre of activity was stationary below the Kangerlussuaq Intrusion with high supply rates, ending with a plumbing system armoured against contamination and the formation of nepheline syenite. As the centre of activity moved southeast towards the rift zone, establishment of new plumbing systems led to a renewed phase of less alkaline, silica-rich and strongly contaminated magmatism.

(4) The final emplacement level of the evolved magmas is related to the degree of crustal contamination. Whereas the most contaminated magmas were emplaced below the plateau basalts, the increasingly less contaminated magmas became ^{18}O-depleted due to stoping into the basalt pile. This could be a consequence of, respectively, increased fractionation and contamination, with resultant higher magma viscosity, causing a less shallow emplacement level, and higher magma supply rate and pressure causing shallower emplacement.

Acknowledgements

This work was part of M. S. Riishuus' Ph.D. project financed by the Science Faculty at the University of Aarhus. Additional financial support was provided by the Danish National Research Foundation through support of the now defunct Danish Lithosphere Centre in Copenhagen. Tod E. Waight, Joel A. Baker and David G. Ulfbeck are thanked for help and technical support with the radiogenic isotope analysis, as is John Lanham for support with the stable isotope spectrometer. Sidsel Grundvig, Ingrid Aaes and Jette Villesen are thanked for their help and technical support with the electron microprobe analyses and thin section preparation. Reviews by J. Godfrey Fitton and G. Nelson Eby helped improve the final product.

References

Ablay, G.J., Carroll, M.R., Palmer, M.R., Mart, J., Sparks, R.S.J., 1998. Basanite–phonolite lineages of the Teide–Pico Viejo volcanic complex, Tenerife, Canary Islands. Journal of Petrology 39, 905–936.

Andreasen, R., Peate, D.W., Brooks, C.K., 2004. Magma plumbing systems in large igneous provinces: inferences from cyclical variations in Palaeogene East Greenland basalts. Contributions to Mineralogy and Petrology 147, 438–452.

Bernstein, S., Leslie, A.G., Higgins, A.K., Brooks, C.K., 2000. Tertiary alkaline volcanics in the Nunatak Region, Northeast Greenland: new observations and comparison with Siberian maymechites. Lithos 53, 1–20.

Bernstein, S., Brooks, C.K., Stecher, O., 2001. Enriched component of the proto-Icelandic mantle plume revealed in alkaline Tertiary lavas from East Greenland. Geology 29, 859–862.

Blichert-Toft, J., Lesher, C.E., Rosing, M.T., 1992. Selectively contaminated magmas of the Tertiary East Greenland macrodike complex. Contributions to Mineralogy and Petrology 110, 154–172.

Brandriss, M.E., Bird, D.K., O'Neil, J.R., Cullers, R.L., 1996. Dehydration, partial melting, and assimilation of metabasaltic xenoliths in gabbros of the Kap Edvard Holm complex, East Greenland. American Journal of Science 296, 333–393.

Breddam, K., 1995. Kærven Gabbro Kompleks; et Tertiært intrusivt bjergartskompleks i Kangerlussuaqområdet, Østgrønland. M.Sc. Thesis, Københavns Universitet.

Brooks, C.K., 1977. Example of magma mixing from the Kialineq district of East Greenland. Bulletin of the Geological Society of Denmark 26, 77–83.

Brooks, C.K., Gill, R.C.O., 1982. Compositional variation in the pyroxenes and amphiboles of the Kangerdlugssuaq intrusion, East Greenland: further evidence for the crustal contamination of syenite magma. Mineralogical Magazine 45, 1–9.

Brooks, C.K., Nielsen, T.F.D., 1982. The Phanerozoic development of the Kangerdlugssuaq area, East Greenland. Meddelelser om Grønland. Geoscience 9, 1–30.

Brooks, C.K., Platt, R.G., 1975. Kaersutite-bearing gabbroic inclusions and the late dike swarm of Kangerdlugssuaq, East Greenland. Mineralogical Magazine 40, 259–283.

Brooks, C.K., Rucklidge, J.C., 1974. Strongly undersaturated Tertiary volcanic rocks the Kangerdlugssuaq area, east Greenland. Lithos 7, 239–248.

Brooks, C.K., Schønwandt, H.K., Stenstrop, G., 1987. Reconnaisance for economic minerals in the Kangerdlugssuaq area, East Greenland. Rapport-Grønlands Geologiske Undersøgelse 135, 66–68.

Brooks, C.K., Tegner, C., Stein, H., Thomassen, B., 2004. Re–Os and ^{40}Ar–^{39}Ar ages of porphyry molybdenum deposits in the East Greenland volcanic rifted margin. Economic Geology 99, 1215–1222.

Brown, P.E., Becker, S.M., 1986. Fractionation, hybridisation and magma mixing in the Kialineq centre, East Greenland. Contributions to Mineralogy and Petrology 92, 57–70.

Brown, P.E., Brown, R.D., Chambers, A.D., Soper, N.J., 1978. Fractionation and assimilation in the Borgtinderne syenite. Contributions to Mineralogy and Petrology 67, 25–34.

Brown, P.E., Evans, I.B., Becker, S.M., 1996. The Prince of Wales Formation—post-flood basalt alkali volcanism in the Tertiary of East Greenland. Contributions to Mineralogy and Petrology 123, 424–434.

Chen, J., Henderson, C.M.B., Foland, K.A., 1994. Open-system, subvolcanic magmatic evolution: constraints on the petrogenesis of the Mount Brome Alkaline Complex, Canada. Journal of Petrology 35, 1127–1153.

Dahlstrøm, K., 1989. Feltgeologiske og petrologisk detaljestudie af Søndre Syenite Gletscher Granit Kompleks (SSGG) i Snout Series, Kangerdlugssuaq, Østgrønland. MSc. Thesis, Københavns Universitet.

Deer, W.A., Kempe, D.R.C., 1976. Geological investigations in East Greenland: Part XI. The minor peripheral intrusions, Kangerdlugssuaq, East Greenland. Meddelelser om Grønland 197, 1–25.

DePaolo, D.J., 1981. Trace element and isotopic effects of combined wallrock assimilation and fractional crystallisation. Earth and Planetary Science Letters 53, 189–202.

Droop, G.T.R., 1987. A general equation for estimating Fe^{3+} concentrations in ferromagnesian silicates and oxides from microprobe analyses, using stoichiometric criteria. Mineralogical Magazine 51, 431–435.

Eldholm, O., Grue, K., 1994. North Atlantic volcanic margins: dimensions and production rates. Journal of Geophysical Research 99, 2955–2968.

Fitton, J.G., Hardarson, B.S., Ellam, R.M., Rogers, G., 1998. Sr-, Nd- and Pb-isotopic composition of volcanic rocks from the southeast Greenland margin at 63°N: temporal variation in crustal contamination during continental breakup. In: Saunders, A.D., Larsen, H.C., WiseJr. Jr., S.W. (Eds.), Proceedings of the Ocean Drilling Program. Scientific Results, vol. 152, pp. 351–358.

Fram, M.S., Lesher, C.E., 1997. Generation and polybaric differentiation of East Greenland early tertiary flood basalts. Journal of Petrology 38, 231–275.

Fujimaki, H., Tatsumoto, M., Aoki, K.-i., 1984. Partition coefficients of Hf, Zr, and REE between phenocrysts and groundmasses. Journal of Geophysical Research 89, 662–672.

Geyti, A., Thomassen, B., 1984. Molybdenum and precious metal mineralization at Flammefjeld, southeast Greenland. Economic Geology 79, 1921–1929.

Goodwin, J.A., Turner, P.A., 1988. East Greenland Kangerdlugssuaq Concession, Summary Report of 1987 Program. Platinova Resources Ltd., Toronto.

Hansen, H., Nielsen, T.F.D., 1999. Crustal contamination in Palaeogene East Greenland flood basalts: plumbing system evolution during continental rifting. Chemical Geology 157, 89–118.

Hansen, H., Pedersen, A.K., Duncan, R.A., Bird, D.K., Brooks, C.K., Fawcett, J.J., Gittins, J., Gorton, M., O'Day, P., 2002. Volcanic stratigraphy of the southern Prinsen af Wales Bjerge region, East Greenland. In: Jolley, D.W., Bell, B.R. (Eds.), The North Atlantic Igneous Province: Stratigraphy, Tectonic, Volcanic and Magmatic Processes. Special Publication-Geological Society of London, vol. 197. Blackwell, Oxford, pp. 183–218.

Harris, C., 1995. Oxygen isotope geochemistry of the Mesozoic anorogenic complexes of Damaraland, northwest Namibia: evidence for crustal contamination and its effect on silica saturation. Contributions to Mineralogy and Petrology 122, 308–321.

Harris, C., Marsh, J.S., Milner, S.C., 1999. Petrology of the alkaline core of the Messum Igneous Complex, Namibia: evidence for the progressively decreasing effect of crustal contamination. Journal of Petrology 40, 1377–1397.

Holm, P.M., 1988. Nd, Sr and Pb isotope geochemistry of the Lower Lavas, E Greenland Tertiary Igneous Province. In: Morton, A.C., Parson, L.M. (Eds.), Early Tertiary volcanism and the opening of the NE Atlantic. Special Publication-Geological Society of London, vol. 39. Blackwell, Oxford, pp. 181–195.

Holm, P.M., 1991. Radiometric age determinations in the Kærven area, Kangerdlugssuaq, East Greenland Tertiary Igneous Province: $^{40}Ar/^{39}Ar$, K/Ar and Rb/Sr isotopic results. Bulletin of the Geological Society of Denmark 38, 183–201.

Holm, P.M., Prægel, N.-O., 1988. The Tertiary Kærven Syenite Complex, Kangerdlugssuaq, East Greenland—mineral chemistry and geochemistry. Mineralogical Magazine 52, 435–450.

Holm, P.M., Prægel, N.-O., 1989. Reply to comments by T.F.D. Nielsen on "The Tertiary Kærven Syenite Complex, Kangerdlugssuaq, East Greenland—mineral chemistry and geochemistry". Mineralogical Magazine 53, 647–651.

Holm, P.M., Prægel, N.-O., 2006-this volume. Cumulates from primitive rifting-related East Greenland Palaeogene magmas: petrological and isotopic evidence from the ultramafic complexes at Kælvegletscher and near Kærven. Lithos 92, 251–275. doi:10.1016/j.lithos.2006.03.036.

Holm, P.M., Prægel, N.-O., Egeberg, E.D., 1991. Mutiple syenite intrusions at Kærven, Kangerdlugssuaq, East Greenland: evidence from the 1986 field work. Bulletin of the Geological Society of Denmark 38, 173–181.

Holm, P.M., Heaman, L.M., Pedersen, L.E., 2006-this volume. U–Pb dating of baddeleyite and zircon: implications for timing of Palaeogene continental breakup in the North Atlantic. Lithos 92, 238–250. doi:10.1016/j.lithos.2006.03.035.

Irvine, T.N., Barager, W.R.A., 1971. A guide to the chemical classification of the common volcanic rocks. Canadian Journal of Earth Sciences 8, 523–548.

Kempe, D.R.C., Deer, W.A., 1970. Geological investigations in East Greenland: Part IX. The mineralogy of the Kangerdlugssuaq alkaline intrusion, East Greenland. Meddelelser om Grønland 190, 1–97.

Kempe, D.R.C., Deer, W.A., 1976. The petrogenesis of the Kangerdlugssuaq alkaline intrusion, East Greenland. Lithos 9, 111–123.

Kempe, D.R.C., Deer, W.A., Wager, L.R., 1970. Geological investigations in East Greenland: Part VIII. The petrology of the Kangerdlugssuaq alkaline intrusion, East Greenland. Meddelelser om Grønland 190, 1–52.

Kyle, P.R., 1981. Mineralogy and geochemistry of a basanite to phonolite sequence at Hut Point peninsula, Antarctica, based on core from Dry Valley Drilling Project drillholes 1, 2 and 3. Journal of Petrology 22, 451–500.

Kyser, T.K., 1986. Stable isotope variations in the mantle. In: Valley, J. W., Taylor Jr., H.P., O'Neil, J.R. (Eds.), Stable Isotopes in High-Temperature Geological Processes. Reviews in Mineralogy, vol. 16. Mineralogical Society of America, Washington, DC, pp. 141–164.

Landoll, J.D., Foland, K.A., Henderson, C.M.B., 1994. Nd isotopes demonstrate the role of contamination in the formation of coexisting quartz and nepheline syenites at the Abu-Khruq complex, Egypt. Contributions to Mineralogy and Petrology 117, 305–329.

Larsen, L.C., 1982. Bagnæsset syenitkompleks, Kangerdlugssuaq Distriktet, Østgrønland. M.Sc. dissertation Thesis, Københavns Universitet.

Larsen, L.M., Watt, W.S., Watt, M., 1989. Geology and petrology of the lower Tertiary plateau basalts of the Scoresby Sund region, East Greenland. Geology of Greenland Survey Bulletin 157, 1–164.

Leake, B.E., Woolley, A.R., Arps, C.E.S., Birch, W.D., Gilbert, M.C., Grice, J.D., Hawthorne, F.C., Kato, A., Kisch, H.J., Krivovichev, V.G., Linthout, K.J.L., Mandarino, J.A., Maresch, W.V., Nickel, E. H., Rock, N.M.S., Schumacher, J.C., Smith, D.C., Stephenson, N. C.N., Ungaretti, L., Whittaker, E.J.W., Youzhi, G., 1997. Nomenclature of amphiboles: report of the Subcommittee on Amphiboles of the International Mineralogical Association, Commission on New Minerals and Mineral Names. Canadian Mineralogist 35, 219–246.

Le Bas, M.J., Streckeisen, A.L., 1991. The IUGS systematics of igneous rocks. Journal of the Geological Society (London) 148, 825–833.

Leeman, W.P., Dasch, E.J., Kays, M.A., 1976. $^{207}Pb/^{206}Pb$ whole-rock ages of gneisses from the Kangerdlugssuaq area, eastern Greenland. Nature 263, 469–471.

Le Maitre, R.W. (Ed.), 1989. A Classification of Igneous Rocks and Glossary of Terms. Blackwell, Oxford. 193 pp.

Lemarchand, F., Villemant, B., Calas, G., 1987. Trace element distribution coefficients in alkaline series. Geochimica et Cosmochimica Acta 51, 1071–1081.

le Roex, A.P., Cliff, R.A., Adair, B.J.I., 1990. Tristan da Cunha, South Atlantic: geochemistry and petrogenesis of a basanite–phonolite lava series. Journal of Petrology 31, 779–812.

Myers, J.S., Gill, R.C.O., Rex, D.C., Charnley, N.R., 1993. The Kap Gustav Holm Tertiary Plutonic Centre, East Greenland. Journal of the Geological Society (London) 150, 259–276.

Nagasawa, H., 1973. Rare-earth distribution in alkali rocks from Oki-Dogo Island, Japan. Contributions to Mineralogy and Petrology 39, 301–308.

Nielsen, T.F.D., 1978. The Tertiary dike swarms of the Kangerdlugssuaq area, East Greenland. An example of magmatic development during continental break-up. Contributions to Mineralogy and Petrology 67, 63–78.

Nielsen, T.F.D., 1980. The petrology of a melilitolite, melteigite, carbonatite and syenite ring dike system in the Gardiner Complex, East Greenland. Lithos 13, 181–197.

Nielsen, T.F.D., 1981. The ultramafic cumulate series, Gardiner Complex, East Greenland—cumulates in a shallow level magma chamber of a nephelinitic volcano. Contributions to Mineralogy and Petrology 76, 60–72.

Nielsen, T.F.D., 1987. Tertiary alkaline magmatism in East Greenland: a review. In: Fitton, J.G., Upton, B.G.J. (Eds.), Alkaline Igneous Rocks. Special Publication-Geological Society of London, vol. 30. Blackwell, Oxford, pp. 489–515.

Nielsen, T.F.D., 1989. Comments on "The Tertiary Kærven Syenite Complex, Kangerdlugssuaq, East Greenland—mineral chemistry and geochemistry". Mineralogical Magazine 53, 647–651.

Nielsen, T.F.D., 2002. Palaeogene intrusions and magmatic complexes in East Greenland, 66 to 75° N. 2002/113, Geological Survey of Denmark and Greenland report 2002/113.

Nielsen, T.F.D., Brooks, C.K., 1991. Generation of nordmarkitic melts by melting of basement gneisses: the Astrophyllite Bay complex, Kangerdlugssuaq. Bulletin of the Geological Society of Denmark 38, 161–164.

Ohja, D.N., 1966. Petrology of the Kærven layered intrusion, east Greenland. Journal-Geochemical Society of India 1, 86–112.

Pankhurst, R.J., Beckinsale, R.D., Brooks, C.K., 1976. Strontium and oxygen isotope evidence relating to the petrogenesis of the Kangerdlugssuaq alkaline intrusion, East Greenland. Contributions to Mineralogy and Petrology 54, 17–42.

Peate, D.W., Stecher, O., 2003. Pb isotope evidence for contributions from different Iceland mantle components to Palaeogene East Greenland flood basalts. Lithos 67, 39–52.

Peate, D.W., Baker, J.A., Blichert-Toft, J., Hilton, D.R., Storey, M., Kent, A.J.R., Brooks, C.K., Hansen, H., Pedersen, A.K., Duncan, R.A., 2003. The Prinsen af Wales Bjerge Formation lavas, East Greenland: the transition from tholeiitic to alkalic magmatism during Palaeogene continental break-up. Journal of Petrology 44, 279–304.

Pedersen, M., 1989. Dannelse af Snout Series og nærliggende magmatiske bjergarter, Kangerdlugssuaq, Østgrønland. MSc Thesis, Københavns Universitet.

Pedersen, A.K., Watt, M., Watt, W.S., Larsen, L.M., 1997. Structure and stratigraphy of the early Tertiary basalts of the Blosseville Kyst, East Greenland. Journal of the Geological Society (London) 154, 565–570.

Philpotts, J.A., Schnetzler, C.C., 1970. Phenocryst-marix partition coefficients for K, Rb, Sr and Ba, with applications to anorthosite and basalt genesis. Geochimica et Cosmochimica Acta 34, 307–322.

Prægel, N.-O., Holm, P.M., 2001. Replenishment episodes and crustal assimilation in the development of an early Tertiary magma chamber, East Greenland: evidence from layered cumulates of the Kælvegletscher ultramafic complex, Kangerlussuaq. Mineralogy and Petrology 73, 279–304.

Prestvik, T., Goldberg, S., Karlsson, H., Grönvold, K., 2001. Anomalous strontium and lead isotope signatures in the off-rift Öræfajökull central volcano in south-east Iceland: evidence for enriched endmember(s) of the Iceland mantle plume? Earth and Planetary Science Letters 190, 211–220.

Riishuus, M.S., Peate, D.W., Tegner, C., Wilson, J.R., Brooks, C.K., Waight, T.E., 2005. Petrogenesis of syenites at a rifted continental margin: origin, contamination and interaction of alkaline mafic and felsic magmas in the Astrophyllite Bay Complex, East Greenland. Contributions to Mineralogy and Petrology 149, 350–371.

Riishuus, M.S., Harris, C., Peate, D.W., Tegner, C., Wilson, J.R., Brooks, C.K., submitted for publication-a. Oxygen and hydrogen isotope geochemistry of the Kangerlussuaq Intrusion, East Greenland: dehydration of basaltic xenoliths with implications for magma differentiation and climate. Contributions to Mineralogy and Petrology.

Riishuus, M.S., Peate, D.W., Tegner, C., Wilson, J.R., Brooks, C.K., submitted for publication-b. The Kangerlussuaq Intrusion revisited: petrogenesis of cogenetic silica over- and under-saturated syenites by periodic recharge in a crustally contaminated magma chamber. Journal of Petrology.

Saunders, A.D., Fitton, J.G., Kerr, A.C., Norry, M.J., Kent, R.W., 1997. The North Atlantic Igneous Province. In: Mahoney, J.J., Coffin, M.F. (Eds.), Large Igneous Provinces: Continental, Oceanic, and Planetary Flood Volcanism. . Geophysical Monograph, vol. 100. American Geophysical Union, Washington, DC, pp. 45–93.

Schnetzler, C.C., Philpotts, J.A., 1970. Partition coefficients of rare earth elements between igneous matrix material and rock-forming mineral phenocrysts—II. Geochimica et Cosmochimica Acta 34, 331–340.

Shimizu, H., 1980. Experimental study on rare-earth element partitioning in minerals formed at 20 and 30 kb for basaltic systems. Geochemical Journal 14, 185–202.

Skovgaard, A.C., 1996. Studie af selektiv skorpekontaminering i kontaktzonen i det tertiære Kærven gabbrokompleks, Kangerlussuaq, Østgrønland og studie af picritiske gange i gabbrokompleksets kontaktzone. M.Sc. Thesis, Københavns Universitet.

Storey, M., Pedersen, A.K., Stecher, O., Bernstein, S., Larsen, H.C., Larsen, L.M., Baker, J.A., Duncan, R.A., 2004. Long-lived postbreakup magmatism along the East Greenland margin: evidence for shallow-mantle metasomatism by the Iceland plume. Geology 32, 173–176.

Taylor, P.N., Kalsbeek, F., Bridgwater, D., 1992. Discrepancies between neodymiun, lead and strontium model ages from the Precambrian of southern East Greenland: evidence for a Proterozoic granulite-facies event affecting Archaean gneisses. Chemical Geology 94, 281–291.

Tegner, C., Duncan, R.A., Bernstein, S., Brooks, C.K., Bird, D.K., Storey, M., 1998a. ^{40}Ar–^{39}Ar geochronology of Tertiary mafic intrusions along the East Greenland rifted margin: relation to flood basalts and the Iceland hotspot track. Earth and Planetary Science Letters 156, 75–88.

Tegner, C., Lesher, C.E., Larsen, L.M., Watt, W.S., 1998b. Evidence from the rare-earth-element record of mantle melting for cooling of the Tertiary Iceland plume. Nature 395, 591–594.

Tegner, C., Brooks, K., Duncan, R.A., Heister, L.E., Bernstein, S., submitted for publication. Protracted Eocene alkaline magmatism in East Greenland linked to rift reorganization on the Iceland hotspot track. Earth and Planetary Science Letters.

Verhoef, J., Roest, W.R., Macnab, R., Arkani-Hamed, J., 1996. Magnetic anomalies of the Arctic and north Atlantic oceans and adjacent land areas. Open File 3125, Geological Survey of Canada.

Villemant, B., 1988. Trace element evolution in the Plegrean Fields, Central Italy: fractional crystallization and selective enrichment. Contributions to Mineralogy and Petrology 98, 169–183.

Villemant, B., Jaffrezic, H., Joron, J.L., Treuil, M., 1981. Distribution coefficients of major and trace-elements—fractional crystallization in the alkali basalt series of Chaine-Des-Puys (Massif Central, France). Geochimica et Cosmochimica Acta 45, 1997–2016.

Vincent, E.A., 1953. Hornblende–lamprophyre dykes of basaltic parentage from the Skaergaard area, East Greenland. Quarterly Journal of the Geological Society of London 109, 21–50.

Wager, L.R., 1947. Geological investigations in East Greenland, Part IV: the stratigraphy and tectonics of Knud Rasmussens Land and the Kangerdlugssuaq region. Meddelelser om Grønland 134, 1–64.

Wager, L.R., 1965. The form and internal structure of the alkaline Kangerdlugssuaq intrusion, East Greenland. Mineralogical Magazine 34, 487–497.